

Assessing The Validity of the Envelope-Function Approximation and the
Effective-Mass Approximation

A Thesis
Presented to
The Division of Mathematics and Natural Sciences
Reed College

In Partial Fulfillment
of the Requirements for the Degree
Bachelor of Arts

Phillip Jahelka

May 2014

Approved for the Division
(Physics)

Darrell Schroeter

Acknowledgements

This thesis wouldn't have been possible without the support from a huge number of people. Incomplete and in no particular order:

My parents for their unwavering support over the years.

Joel Brand for mentoring me during my early years, providing incredible support for my numerous science projects, and Thai food.

John MacFarlane for nurturing my interest in physics during high school and putting up with me during Science Olympiad.

My friends; especially Allie Hemmings, Grahame Watt, and Mark Walth, for being comrades in arms over these four years and helping to keep me sane.

My advisor, Johnny Powell, for his wonderful support and encouragement.

And finally Darrell Schroeter for making this thesis the most engaging and stimulating project of my life.

It takes a village to write a thesis

Olde Outhaüs Proverb

Table of Contents

Introduction	1
Quantum Dots	1
Quantum Dot Model	3
Chapter 1: Exact Solution	11
1.1 Introduction	11
1.2 Determining the Wave Function in Adjacent Regions	11
1.3 Boundary Conditions	13
1.3.1 Zero Boundary Conditions	13
1.3.2 Periodic Boundary Conditions	13
1.4 Useful Results	14
1.4.1 Speeding up Computation of $\mathbb{P}\mathbb{T}$	14
1.4.2 Properties of $\mathbb{P}\mathbb{T}$	17
Chapter 2: The Classic Solution	19
2.1 Introduction	19
2.2 Bloch's Theorem	19
2.3 Useful Concepts from Solid State Physics	21
2.3.1 Quasi-Momentum	21
2.3.2 Effective Mass	22
2.4 The Kronig-Penney Model	23
2.4.1 Method Validation	26
2.5 The Envelope-Function Approximation	26
2.6 The Effective-Mass Approximation	30
Chapter 3: Results	33
3.1 Applying Solution Methods	33
3.1.1 Exact Method	33
3.1.2 Envelope-Function Approximation	35
3.2 Effective-Mass Approximation	36
3.3 Building the Model	37
3.3.1 Units	37
3.3.2 Kronig-Penney Parameters	37
3.3.3 Perturbation Parameters	38
3.4 Results	38

3.4.1	Constant Perturbation Only	39
3.4.2	Lattice Constant Perturbation Only	40
3.4.3	Both Perturbations	43
3.4.4	General Comments	44
Chapter 4:	Conclusion	49
Appendix A:	Proof of Unimodular Matrix Power Formula	51
Appendix B:	Annotated Code	53
B.1	General Calculation	53
B.2	Manipulating Potentials	54
B.3	Calculating $r(E)$	56
B.4	Numerics	57
B.5	Kronig-Penney	58
B.6	Building Functions	59
References		61

List of Tables

1	An example of the algorithm for subtracting potentials. The first line is just the inputs. Each line after that represents an iteration of the algorithm. It terminates when both lists used for generating the difference are empty.	7
3.1	Results for case of constant perturbation only.	39
3.2	Results for case of only perturbed lattice constant.	40
3.3	Results for case of both perturbations applied.	43
3.4	These are the strengths of the Dirac delta potentials that kink the envelopes and wave functions of the EMA. Subscripts indicate if it's the kink of an envelope or wave function and if it's the kink at the left or right end of the perturbation.	44

List of Figures

1	This is a simple schematic of a molecular beam epitaxy Device. In, Ga, and As correspond to Indium, Gallium and Arsenic furnaces, respectively. The substrate material is GaAs and the deposited material is represented as triangles to give the impression of the deposited InGaAs layer breaking up into islands and forming quantum dots.	2
2	This plot shows the conduction band edge along the growth axis of a material containing a quantum dot. Because the band edge in the dot is lower than in the bulk material, electrons excited to the conduction band in the dot will be strongly localized. States above the band edge are allowed. The vertical scale is energy.	2
3	Simple example of a one-dimensional piecewise-constant potential. . .	4
4	Unperturbed potential.	4
5	An example of the full potential. In this case, we've picked $\gamma < 1$, and $U_p < 0$. In an actual model, there would be several dozen unit cells total.	6
6	This is an example potential to demonstrate my notation. This example would be notated as $((1, 1), (1.5, 3), (1, 2)$	7
7	These three potentials represent the difference calculated in Table 1. The third plot added to the second would reproduce the first.	8
8	Potential used for the effective-mass approximation.	9
9	An example perturbing potential for the quantum dot model. There are two important things to note about this potential. First, is that it clearly has large high-frequency Fourier components, directly contradicting the assumptions of the EFA. Second, is that it's non-periodic and we don't know its closed form expression.	9
1.1	Sample potential for establishing continuity relations.	12
1.2	The purpose of this figure is to illustrate how Eq. 1.21 works. The system consists of two types of unit cells with three of the first kind and two of the second. The arrows represent how the various matrices shift coefficients. The $(T_i)^{y_i-1}$ are responsible for moving the coefficients through a large number of unit cells quickly, and the S_i enforce continuity at the border between different unit cells.	16

2.1	The last two terms of Eq. 2.45. Where the magnitude of the function exceeds one, a real k does not exist. The regions where k does exist are called bands and the regions where it doesn't are bandgaps.	24
2.2	The solutions to Eq. 2.45 plotted as a dispersion relation. The most important feature of this plot is that the bandgaps alternate between occurring at $k = 0$ and $k = \pi/a$	25
2.3	The exact method and Kronig-Penney agree on the band edges of a series of square wells. The yellow shaded regions are bandgaps and the downward spikes represent allowed states. Also, because the exact method doesn't have a wave vector argument, it finds all allowed states.	26
2.4	Example potential used for deriving envelope-function boundary conditions for the effective-mass approximation.	31
3.1	This graphical derivation of PT for the exact potential is analogous to Fig. 1.2.	34
3.2	Demonstration that it's possible to miscalculate the sign of the derivative which can cause the bisection routine to converge to a value outside the error tolerance of the actual root.	35
3.3	The bandstructure of Silicon is fairly complicated because it's an indirect bandgap semiconductor meaning the bandgap isn't due to band edges that are aligned in k -space. However, if we imagine shifting the bands so that it was a direct bandgap material like Kronig-Penney, then the Silicon bands would most closely correspond to the second and third Kronig-Penney bands[19].	38
3.4	The calculated Kronig-Penney wave function for the model over 4 unit cells. It's exactly what one would expect: a travelling wave periodic in the lattice.	39
3.5	The top wave function is the amplitude of the third wave function predicted by the EFA in the case of only constant perturbation. It's arguable this wave function isn't strongly localized because its confinement measure is less than 0.5. Nevertheless, we count it because the wave function does not have a maxima in the unperturbed region and if the length of the unperturbed region were increased the confinement measure would also increase. The bottom wave function is the next excited state to show that the localized and non-localized wave functions are qualitatively different.	41
3.6	The predicted wave functions for the case of $U_p = 0$ and $\gamma = 1.05$. . .	42
3.7	These are the predicted envelope-functions of the EFA and EMA for the model with $U_p = -0.02$ and $\gamma = 1.05$. Notice how the EFA has high-frequency oscillations on top of the envelope and both exhibit less confinement as they increase in energy.	45

- 3.8 These are the shared predicted wave functions of the exact solution, EFA, and EMA for the model with $U_p = -0.02$ and $\gamma = 1.05$. Notice how with each energy increase a node in the envelope is added in the perturbed region. Also, we can qualitatively see how badly the EFA and EMA estimate confinement for the third state.
- 3.9 These are the higher-energy states that the EFA and EMA fail to predict. We can see how even these high-energy states are nearly as confined as the second states predicted by the EFA and EMA. . . .

46

47

Abstract

The envelope-function approximation (EFA) and the effective-mass approximation (EMA) were compared to an exact solution for a perturbed Kronig-Penney model. The EFA and EMA were found to underestimate both the number of localized states and the extent to which wave functions are confined to the perturbed region. The exact solution predicted five localized states compared to three for both the EFA and the EMA. The predicted confinements of the exact solution were 99%, 96%, 92%, 88%, and 80%, in order of increasing energy. The predicted confinements of the EFA were 97%, 90%, and 62% and 97%, 88%, and 53% for the EMA, again in order of increasing energy. EFA and EMA also both overestimated energies of allowed states. The EFA overestimated by 10%, 10%, and 9.6%, and the EMA by 11%, 11%, and 10%, again in order of increasing energy. The envelope-function approximation was found to be more accurate than the effective-mass approximation.

Introduction

Quantum Dots

Quantum dots are semiconductor structures that exhibit quantum confinement[1]. Confinement means that an electron excited to the conduction band of the dot will remain inside the dot. There are two main types of quantum dots: colloidal and heterostructure[2]. Colloidal quantum dots are small semiconductor crystals suspended in solution. Heterostructure quantum dots consist of small impurities in a semiconductor substrate. This thesis focuses on heterostructure-type dots.

One common method to construct semiconductor heterostructures is molecular beam epitaxy (MBE). Using MBE, experimenters can grow semiconductors one layer at a time by depositing semiconductor layers on top of a substrate[3]. This is accomplished by placing a substrate in ultra-high vacuum (10^{-8} Pa) in close proximity to furnaces containing the materials to be deposited on the substrate. As furnace temperature increases, some of the material sublimates and is deposited on the substrate. By controlling furnace temperature and orifice size, extreme control can be achieved of the crystals being grown on the substrate. A rough diagram of an MBE apparatus is shown in Fig. 1.

MBE can be used to grow semiconductor heterostructures by alternating which materials are being deposited on the substrate. This technique can be used to make quantum dots by first growing GaAs, and then depositing a thin layer of InGaAs. The lattice constants of GaAs and InGaAs are not perfectly matched which introduces strain in the InGaAs layer. Under sufficient strain, the InGaAs layer breaks up and forms nanometer scale islands. These islands form the quantum dots. Finally, they are capped with another layer of GaAs.

To see that electrons would be confined to the dot, consider the lowest allowed energy of the conduction band, also known as the conduction band edge, as a function of the growth axis, shown in Fig. 2[4]. The difference between the conduction band edges, also known as the conduction band offset, between GaAs and $\text{Ga}_{0.47}\text{In}_{0.53}\text{As}$ is on the order of -0.6 eV[5]. This means that the InGaAs impurity acts like a finite square well for electrons in the conduction band, binding electrons with energy less than the conduction band edge of the GaAs.

This complex electronic structure makes quantum dots an attractive tool for advancing everything from standard semiconductor devices using heterostructures to molecular tagging for biology using colloidal quantum dots[6][7]. In order for these applications to be realized, we need a good understanding of electron behavior in

Figure 1: This is a simple schematic of a molecular beam epitaxy Device. In, Ga, and As correspond to Indium, Gallium and Arsenic furnaces, respectively. The substrate material is GaAs and the deposited material is represented as triangles to give the impression of the deposited InGaAs layer breaking up into islands and forming quantum dots.

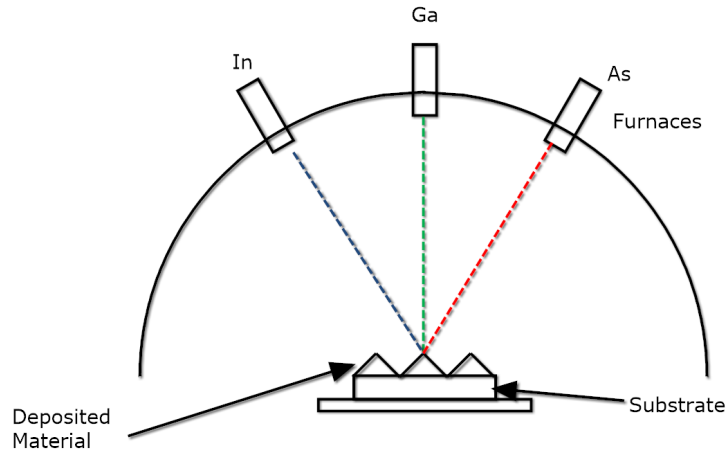
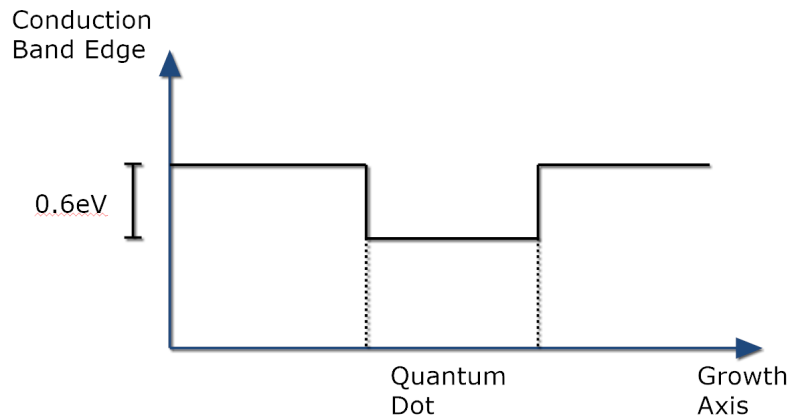


Figure 2: This plot shows the conduction band edge along the growth axis of a material containing a quantum dot. Because the band edge in the dot is lower than in the bulk material, electrons excited to the conduction band in the dot will be strongly localized. States above the band edge are allowed. The vertical scale is energy.



quantum dots. The purpose of this thesis is to evaluate the accuracy of the standard methods for determining energy eigenstates of electrons confined to a quantum dot.

The most correct way to calculate the wave function of an electron in a crystal is to perform a pseudopotential calculation where the effects of the nuclei and other electrons are lumped into an effective potential that the electron experiences[8]. These calculations are challenging enough for a bulk material and the reduced symmetry due to the quantum dot makes them extremely difficult. But, if you assume that the quantum dot, the InGaAs in the above example, is a small, slowly varying perturbation to the lattice, an approximate solution may be found using either the envelope-function approximation (EFA) or the effective-mass approximation (EMA)[9]. It's not clear if these approximations are reasonable. First, the perturbation is not slowly varying in two ways: the border between the substrate and the dot is abrupt; it is not ambiguous if an atom is part of the substrate or dot, and the materials don't have the same lattice constant, so if the dot is treated as a perturbation it will have large, high-frequency Fourier components because of the sharp boundary. In addition, the difference of lattice constants between InGaAs and GaAs can be as large as 5%[10] which will also introduce large high-frequency components to the perturbation. Secondly, if we take the natural energy scale to be set by the GaAs bandgap of 1.424eV, and the perturbation strength to be the band offset at 0.6 eV, then the perturbation covers almost half of the energy scale, suggesting it's not "small." The other method commonly used to solve for the energy eigenstates is the effective-mass approximation (EMA)[11]. The EMA assumes that system can be treated as the junction of two bulk materials. This assumption doesn't appear valid for quantum dots because the size of a dot is on the order of ten to a hundred atoms; nowhere near large enough for it to seem like a bulk material[2].

The purpose of this thesis is to determine how well the EFA and EMA approximate the actual wave functions and energies in a quantum dot. This problem is extremely difficult for the full system in three dimensions, so we construct a much simpler one-dimensional model that can be solved, up to numerical errors, using both the EFA, EMA, and an exact method. We then compare their predictions.

Quantum Dot Model

In order to test how well the EFA and EMA predict wave functions in quantum dots, we must construct a model that is both simple enough to solve exactly, but still be sufficiently complex to resemble a quantum dot. To satisfy the simplicity requirement, we work in one dimension with a piecewise-constant potential; an example of such a potential is in Fig. 3. Working in one dimension eliminates most of the degeneracy (left and right traveling waves are still degenerate, for example), and requiring the potential be piecewise constant is useful because the solution to the Schrödinger equation for a constant potential is known. Finally, we use periodic boundary conditions which allow for traveling wave solutions and will maintain consistent boundary conditions between the EFA, EMA, and the exact solution.

The unperturbed system is supposed to model a perfect lattice. Along with the

Figure 3: Simple example of a one-dimensional piecewise-constant potential.

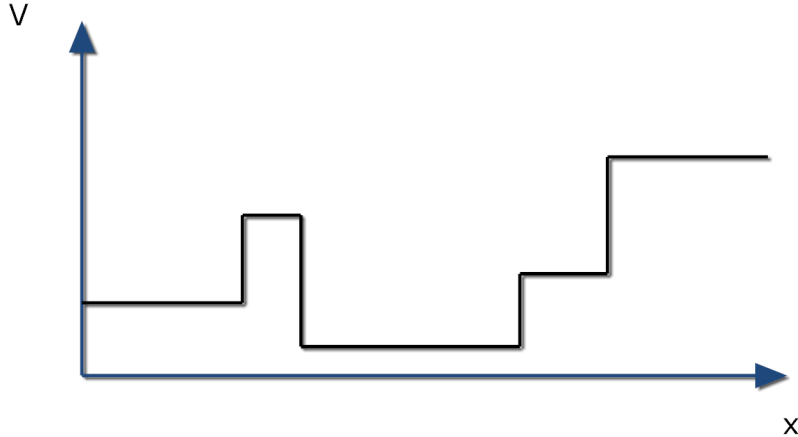
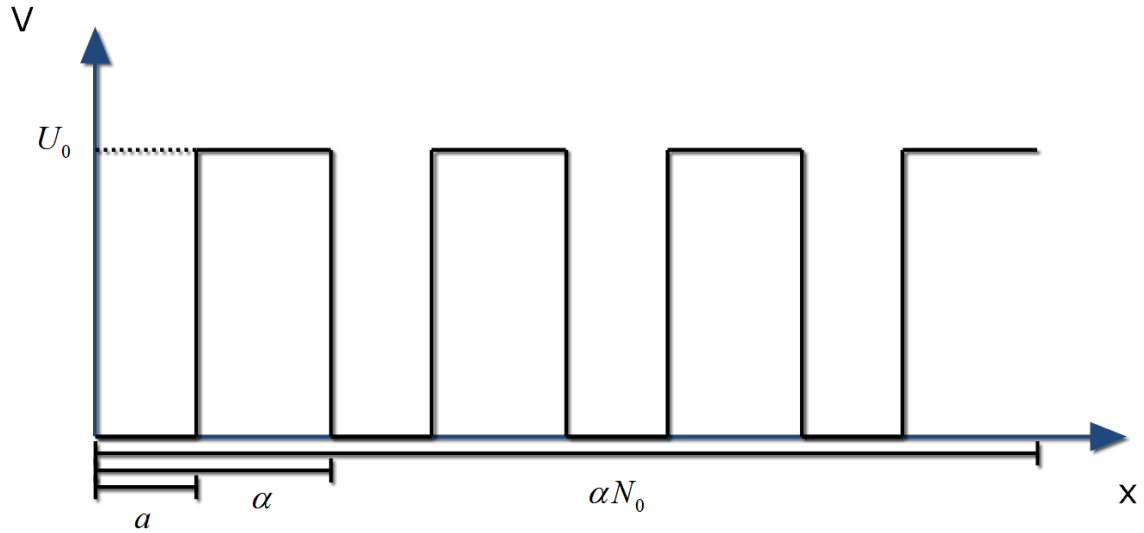


Figure 4: Unperturbed potential.



requirement that the potential be piecewise constant, the simplest unperturbed potential is therefore a series of square wells. The unperturbed system is characterized by the number of wells, N_0 , the distance between them α the length of a low potential region a and the height of the high potential regions, U_0 . Without loss of generality, we take the low potential regions to have $V = 0$ and that the first region is one of low potential. The unperturbed potential is illustrated in Fig. 4. The high-potential regions are supposed to represent regions between ions while the low potential regions are ion cores or nuclei.

There are two ways the lattice can be perturbed to make it resemble a quantum dot. First, it can have its potential changed by a constant for some length. Secondly, the perturbed part of the lattice can have a different lattice constant. These two perturbations are completely described by the number of perturbed cells N_p the proportionality constant linking the unperturbed lattice constant to the perturbed γ

so that $\alpha' = \gamma\alpha$ and $a' = \gamma a$, and the amount by which the potential is shifted U_p . The convention is made that the perturbation occurs on the “left” side of the system. One issue with this specification is that the perturbed and unperturbed lattices are not guaranteed to exactly meet up. To see this, consider that the length of the perturbation $\alpha\gamma N_p$ is not necessarily an integer multiple of α . To remedy this, the perturbation is extended by:

$$\Delta \equiv N_0\alpha - N_p\gamma\alpha - \alpha\lfloor N_0 - \gamma N_p \rfloor \quad (1)$$

and the potential associated with this part of the perturbation is 0. An example is shown in Fig. 5.

In order to apply the EFA, you need to be able to write down the potential that when added to the unperturbed system will produce the perturbed system. Calculating the perturbation is equivalent to subtracting the unperturbed system from the perturbed. To do this, we first need some notational tools.

While piecewise-constant potentials could be written using summation notation and Heaviside step functions, we instead use a custom notation to describe them. The notation consists of an ordered list of ordered pairs. The elements of the list directly correspond, in order, to a part of the potential. The first element of each ordered pair is the length of an area of constant potential, and the second element of the ordered pair corresponds to the value of the potential itself. For an example, see Fig. 6. Also, we refer to any ordered pair as a “region.” These lists for the model are arbitrarily long, but are also very repetitive. To compress these lists we use the symbols “ \times ” and “ $+$ ” which refer to repeating some list of ordered pairs and concatenating a list, respectively. For example,

$$((3, 5), (3, 5), (3, 5), (4, 7), (4, 7)) \equiv ((3, 5)) \times 3 + ((4, 7)) \times 2. \quad (2)$$

Furthermore, we refer to the object on the left-hand side of a “ \times ” as a unit cell.

With this notation in mind, the potential of the unperturbed lattice is written:

$$((a, 0), (\alpha - a, U_0)) \times N_0, \quad (3)$$

and that of the the perturbed lattice is written:

$$((\gamma a, U_p), (\gamma(\alpha - a), U_0 + U_p)) \times N_p + ((\Delta, 0)) + ((a, 0), (\alpha - a, U_0)) \times \lfloor N_0 - \gamma N_p \rfloor. \quad (4)$$

We can now describe an algorithm for determining the perturbing potential the EFA takes as its argument; the explanation is most clear using an example. Suppose you want to subtract, in the physical sense, $((1, 2), (3, 4))$ from $((2, 4), (2, 6))$. First, you compare the first elements of each list. The potential of the first element of the difference is the difference of the potentials; 2 in this case. The length of the first element of the difference is the length of the shorter of the two elements; 1 for this example. The length of the shorter region is then subtracted from the length of the longer region and the ordered pair of the shorter region is deleted. If the lengths are the same, they are both deleted. This procedure is iterated until both lists used to calculate the difference are empty. This example is fully worked out in Table 1 and

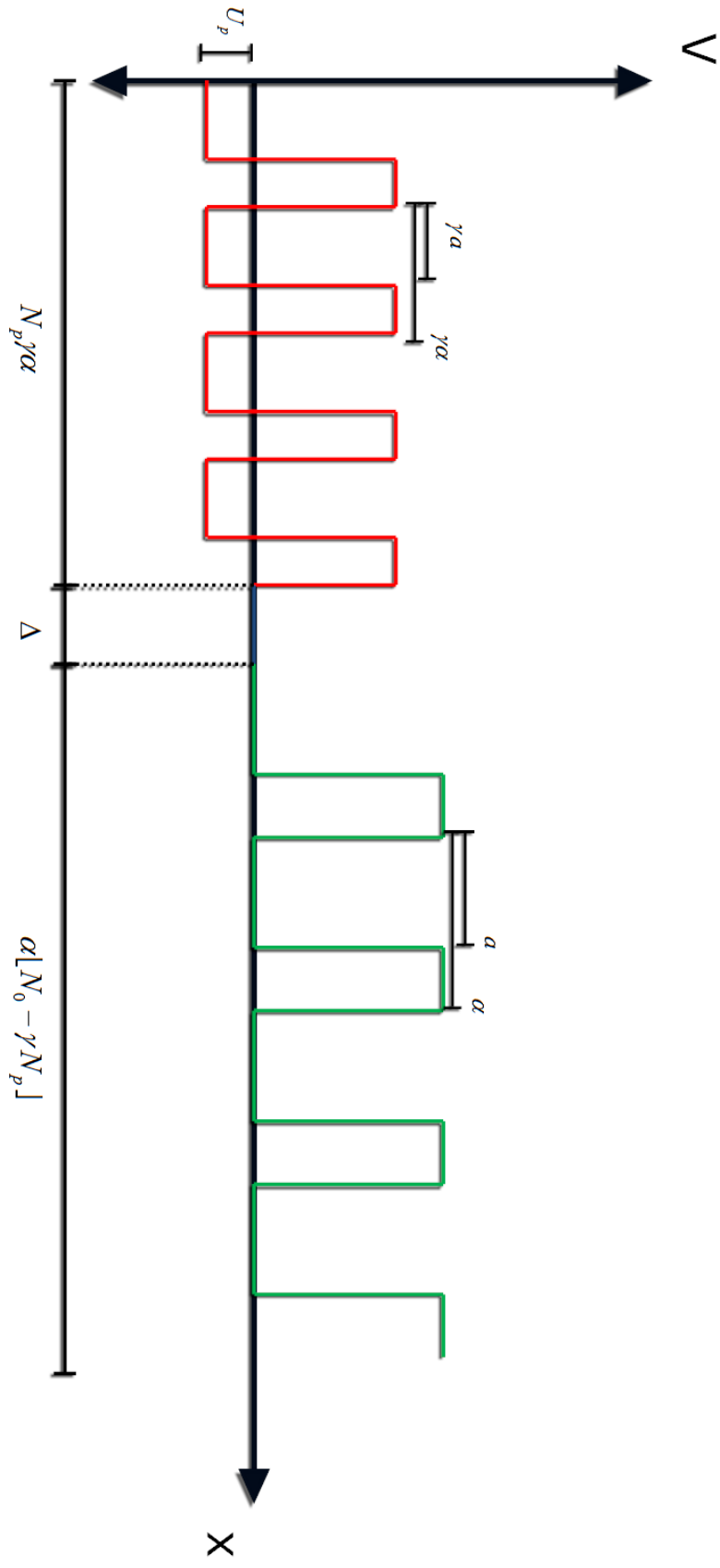


Figure 5: An example of the full potential. In this case, we've picked $\gamma < 1$, and $U_p < 0$. In an actual model, there would be several dozen unit cells total.

Figure 6: This is an example potential to demonstrate my notation. This example would be notated as $((1, 1), (1.5, 3), (1, 2))$

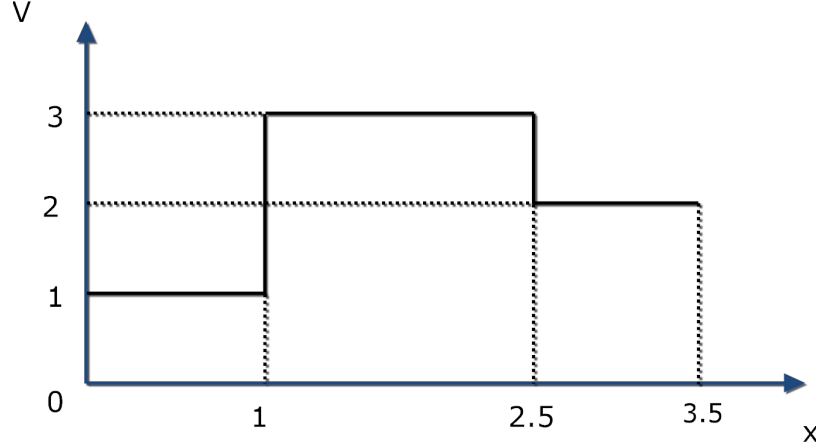


Table 1: An example of the algorithm for subtracting potentials. The first line is just the inputs. Each line after that represents an iteration of the algorithm. It terminates when both lists used for generating the difference are empty.

Step	V_1	V_2	$V_1 - V_2$
0	$((2, 4), (2, 6))$	$((1, 2), (3, 4))$	$()$
1	$((1, 4), (2, 6))$	$(3, 4))$	$((1, 2))$
2	$(2, 6))$	$(2, 4))$	$((1, 2), (1, 0))$
3	$()$	$()$	$((1, 2), (1, 0), (2, 2))$

the associated potentials are shown in Fig. 7. This algorithm will generally return adjacent regions with the same potential, so the last step is joining adjacent regions with the same potential to make the representation of the potential as compact as possible.

Applying this to the algorithm to the perturbed and unperturbed systems returns the perturbation the EFA uses. An example perturbing potential for the EFA is shown in Fig. 9.

The potential for the EMA is constructed using a much more heuristic argument. The potential of the perturbation is simply U_p , but it also admits a spatially varying effective mass. The idea is the U_p captures the average perturbed potential, while the two different masses contains the perturbed lattice constant. For this model, we define Δ to be part of the unperturbed lattice. An example potential is shown in Fig. 8.

Having formally stated the problem we solve, my thesis proceeds as follows. First, we derive a method for solving these types of potentials exactly and then motivate and derive the EFA and EMA. Next, we explain in detail how to apply these methods to the quantum dot model, and motivate the parameters we choose for the model. Finally, we solve the model using the three methods and compare the results.

Figure 7: These three potentials represent the difference calculated in Table 1. The third plot added to the second would reproduce the first.

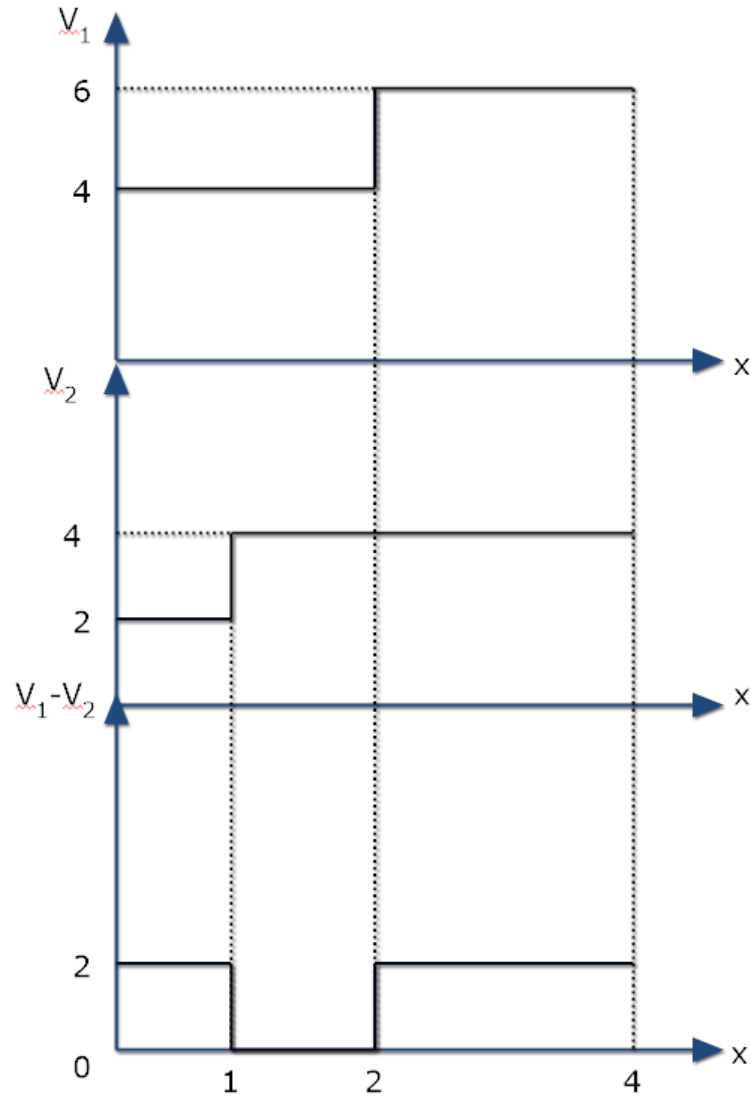


Figure 8: Potential used for the effective-mass approximation.

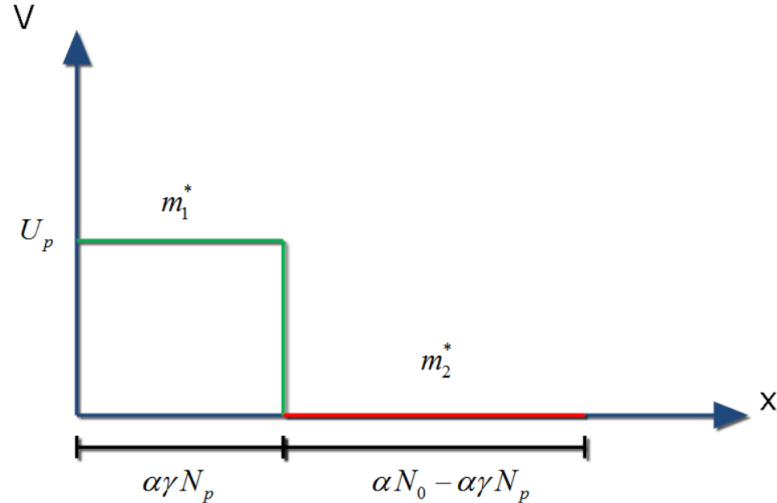
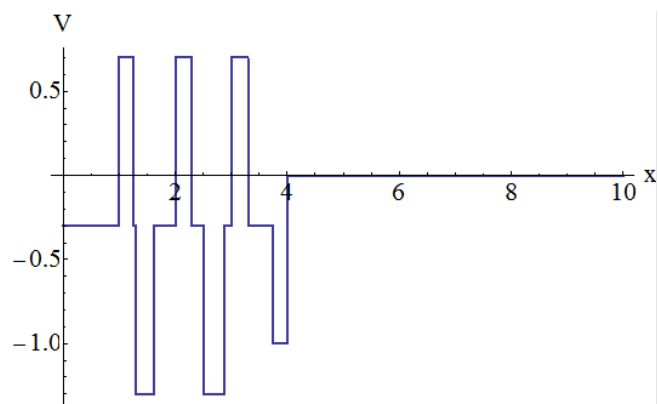


Figure 9: An example perturbing potential for the quantum dot model. There are two important things to note about this potential. First, is that it clearly has large high-frequency Fourier components, directly contradicting the assumptions of the EFA. Second, is that it's non-periodic and we don't know its closed form expression.



Chapter 1

Exact Solution

1.1 Introduction

The purpose of this chapter is to outline a general method for finding the energies and wave functions of arbitrary piecewise-constant potentials. The method is developed for either zero or periodic boundary conditions. Finding allowed energies and wave functions is accomplished by using the known solution to the Schrödinger equation in a region of constant potential and then using continuity relations to determine the wave function in adjacent regions. If the wave function is required to be zero at the boundaries, the computational problem can be stated as a simple shooting problem. If, however, the wave function is required to be periodic on the boundary then a couple intermediate steps of linear algebra are required before the problem can be stated in a form susceptible to numerical methods.¹

1.2 Determining the Wave Function in Adjacent Regions

To develop a general method for finding the energies and wave functions of an arbitrary, piecewise-constant potential, consider two adjacent regions of possibly different potential; see Fig. 1.1. If we take the origin of the coordinate system to be the left-hand side of the system, the wave function in two neighboring regions can be written as

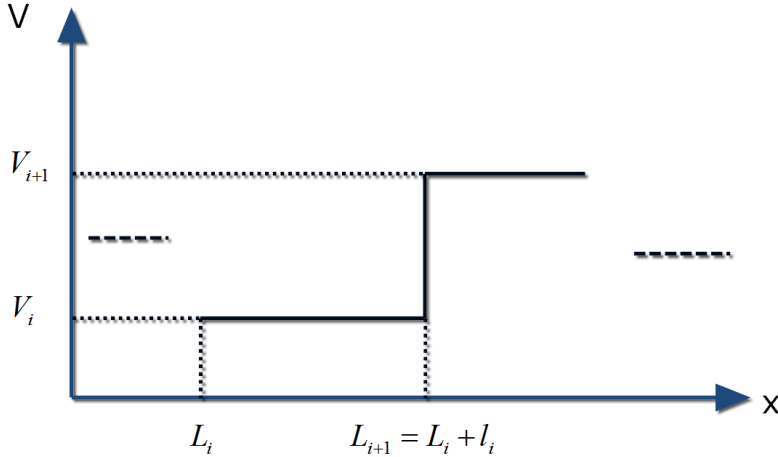
$$\psi(x) = \begin{cases} A_i e^{ik_i(x-L_{i-1})} + B_i e^{-ik_i(x-L_{i-1})} & : L_{i-1} < x < L_i \\ A_{i+1} e^{ik_{i+1}(x-L_i)} + B_{i+1} e^{-ik_{i+1}(x-L_i)} & : L_i < x < L_{i+1} \end{cases}, \quad (1.1)$$

where

$$k_i \equiv \frac{\sqrt{2m(E - V_i)}}{\hbar} \quad (1.2)$$

¹This method is strongly inspired by Griffiths and Steinke, 2001 [12].

Figure 1.1: Sample potential for establishing continuity relations.



and

$$L_i \equiv \sum_{j=1}^i l_j \quad (1.3)$$

with $L_0 \equiv 0$. If we demand continuity of $\psi(x)$ and its derivative at the boundary of the two regions; at L_{i+1} in Fig. 1.1, we can find A_{i+1} and B_{i+1} as functions of A_i and B_i . In fact, it can be expressed by the following matrix relationship:²

$$\begin{pmatrix} A_{i+1} \\ B_{i+1} \end{pmatrix} = \frac{1}{2k_{i+1}} \begin{pmatrix} e^{il_i k_i} (k_i + k_{i+1}) & e^{-il_i k_i} (-k_i + k_{i+1}) \\ e^{il_i k_i} (-k_i + k_{i+1}) & e^{-il_i k_i} (k_i + k_{i+1}) \end{pmatrix} \begin{pmatrix} A_i \\ B_i \end{pmatrix}. \quad (1.4)$$

If we make the identification

$$\mathbb{M}_i \equiv \frac{1}{2k_{i+1}} \begin{pmatrix} e^{il_i k_i} (k_i + k_{i+1}) & e^{-il_i k_i} (-k_i + k_{i+1}) \\ e^{il_i k_i} (-k_i + k_{i+1}) & e^{-il_i k_i} (k_i + k_{i+1}) \end{pmatrix}, \quad (1.5)$$

it's clear by induction that

$$\begin{pmatrix} A_{i+j} \\ B_{i+j} \end{pmatrix} = \prod_{k=i}^{j-1} \mathbb{M}_k \begin{pmatrix} A_i \\ B_i \end{pmatrix}. \quad (1.6)$$

For convenience, we make the definition:

$$\mathbb{T} \equiv \prod_{k=1}^{N-1} \mathbb{M}_k, \quad (1.7)$$

where N is the number of regions in the system, so that

$$\begin{pmatrix} A_N \\ B_N \end{pmatrix} = \mathbb{T} \begin{pmatrix} A_1 \\ B_1 \end{pmatrix}. \quad (1.8)$$

²If this calculation is not familiar, refer to Sections 2.5 and 2.6 and problems 2.52 and 2.53 of D. Griffith's *Introduction to Quantum Mechanics*[13].

What Eq. 1.6 means is that if the coefficients of the wave function in any region are known then they can be found for the rest of system by multiplying them by \mathbb{M} matrices or their inverses. Therefore, the problem is finding energies, which are buried in the k 's, such that the wave function satisfies the imposed boundary conditions. The next step is imposing boundary conditions.

1.3 Boundary Conditions

In this section, we first look at how to enforce zero boundary conditions and secondly at periodic boundary conditions. After this section we will assume periodic boundary conditions to maintain continuity with the EFA and EMA. The case of zero boundary conditions is presented due to their simplicity and usefulness in a wide variety of other problems.

1.3.1 Zero Boundary Conditions

Zero boundary conditions are characterized by:

$$\psi(0) = 0 \quad \psi(L_N) = 0. \quad (1.9)$$

These boundary conditions are chosen when modeling a quantum mechanical system in a “box.” To impose them, consider that the conditions requires both

$$A_1 + B_1 = 0 \quad A_N e^{ik_N l_N} + B_N e^{-ik_N l_N} = 0. \quad (1.10)$$

These conditions can be expressed as

$$(1 \quad 1) \begin{pmatrix} A_1 \\ B_1 \end{pmatrix} = 0 \quad (e^{ik_N l_N} \quad e^{-ik_N l_N}) \mathbb{T} \begin{pmatrix} A_1 \\ B_1 \end{pmatrix} = 0 \quad (1.11)$$

At the cost of the wave function being *a priori* normalized, we can choose one of the coefficients. With the choice $A_1 = 1$, it's then required that $B_1 = -1$. With this choice, the first half of Eq. 1.10 is obviously satisfied and we can now calculate numerical values for A_N and B_N . Therefore, the goal becomes finding energies such that

$$(e^{ik_N l_N} \quad e^{-ik_N l_N}) \mathbb{T} \begin{pmatrix} 1 \\ -1 \end{pmatrix} = 0. \quad (1.12)$$

1.3.2 Periodic Boundary Conditions

Periodic boundary conditions take the form

$$\psi(0) = \psi(L_N) \quad \psi'(0) = \psi'(L_N). \quad (1.13)$$

One way to proceed is to write down the functional form of the wave function in the first and last region and work the algebra until obtaining a useful result. However, the matrix method presents a very concise way of solving the problem. Consider an

\mathbb{M}_i matrix, call it \mathbb{P} , such that it shifts the coefficients from the N^{th} region to the first. Using an \mathbb{M}_i matrix to enforce periodic boundary conditions is a valid strategy because the continuity conditions that the \mathbb{M}_i enforce agree with periodic boundary conditions. We then have the relationships

$$\begin{pmatrix} A_N \\ B_N \end{pmatrix} = \mathbb{T} \begin{pmatrix} A_1 \\ B_1 \end{pmatrix} \quad (1.14)$$

$$\begin{pmatrix} A_1 \\ B_1 \end{pmatrix} = \mathbb{P} \begin{pmatrix} A_N \\ B_N \end{pmatrix} \quad (1.15)$$

where,

$$\mathbb{P} \equiv \frac{1}{2k_1} \begin{pmatrix} e^{il_N k_N} (k_N + k_1) & e^{-il_N k_N} (-k_N + k_1) \\ e^{il_N k_N} (-k_N + k_1) & e^{-il_N k_N} (k_N + k_1) \end{pmatrix}, \quad (1.16)$$

which can be combined to give

$$\begin{pmatrix} A_1 \\ B_1 \end{pmatrix} = \mathbb{P} \mathbb{T} \begin{pmatrix} A_1 \\ B_1 \end{pmatrix}. \quad (1.17)$$

It's now clear that enforcing periodic boundary conditions is an eigenvalue problem; finding energies such that an eigenvalue of $\mathbb{P}\mathbb{T}$ is 1. Finding eigenvalues is accomplished with rootfinding on the characteristic equation for eigenvalues with the assumption the eigenvalue is one:

$$\det(\mathbb{P}\mathbb{T} - \mathbb{I}) = 0, \quad (1.18)$$

where \mathbb{I} is the identity matrix. Once a root is found, an eigenvector of $\mathbb{P}\mathbb{T}$ gives the values of A_1 and B_1 . The wave function is then constructed by propagating these coefficients using the \mathbb{M}_i matrices.

1.4 Useful Results

The method described will solve the Schrödinger equation for any piecewise-constant potential, but it is hampered by a possible over-abundance of linear algebra and requiring a large number of matrix-matrix multiplications to compute $\mathbb{P}\mathbb{T}$. It turns out that the linear algebra can be further simplified and that a couple methods can significantly speed up calculating $\mathbb{P}\mathbb{T}$.

1.4.1 Speeding up Computation of $\mathbb{P}\mathbb{T}$

The method described in Sec. 1.3.2 is hampered by requiring a large number of matrix multiplications, making the computation fairly slow. Nevertheless, if the potential is weakly periodic then the method can be reduced to a small number of matrix-matrix multiplications. By weakly periodic we mean that the representation of the potential benefits from being written in the form

$$\sum_{i=1}^s U_i \times y_i, \quad (1.19)$$

where s is the number of different kinds of unit cells, including multiplicity if the same unit cells appears at different points in the system, U_i are the unit cells, and the y_i are how many times each unit cell is repeated.

The first thing to notice is that the \mathbb{M}_i matrices in Eq. 1.5 don't depend on the distance to the origin. This translational symmetry means that individual \mathbb{M}_i and their products can be reused when constructing \mathbb{T} .

To make use of this observation, we first define

$$\mathbb{T}_i = \prod_{m=1}^{j-1} \mathbb{M}_{m,i} \quad (1.20)$$

where $\mathbb{M}_{m,i}$ is the matrix that shifts the coefficients from the m^{th} region of the i^{th} type of unit cell to the next region and j is the number of regions in the unit cell. These can be thought of as miniature \mathbb{T} matrices particular to one kind of unit-cell. In particular the \mathbb{PT} matrix associated with the potential in Eq. 1.19 is:

$$\mathbb{PT} = \sum_{i=s}^1 \mathbb{S}_i \mathbb{T}_i (\mathbb{P}_i \mathbb{T}_i)^{y_i-1}, \quad (1.21)$$

where \mathbb{P}_i is the \mathbb{M}_i that shifts the coefficients from the last to the first region of the i^{th} type of unit cell, \mathbb{S}_i is the \mathbb{M}_i that propagates the coefficients from the last region of the i^{th} type of unit cell to the first region of the next type, and $\mathbb{S}_s \equiv \mathbb{P}$. The \mathbb{S}_i can be thought of as stitching together the various types of unit cells. Although this formula is not as clean as simply evaluating a large product, it significantly reduces the amount of computation that must be done if a unit cell contains a large number of regions. To see this formula in action, refer to Fig. 1.2.

The second useful result allows us to further simplify the computation if y_i is large. First, we evaluate the determinant of an \mathbb{M}_i matrix from Eq. 1.5:

$$\det(\mathbb{M}_i) = \frac{1}{4k_{i+1}^2} ((k_i + k_{i+1})^2 - (k_i - k_{i+1})^2) = \frac{k_i}{k_{i+1}}. \quad (1.22)$$

From Eq. 1.22, it immediately follows that

$$\det \left(\prod_{k=i}^j \mathbb{M}_k \right) = \frac{k_i}{k_j} \quad (1.23)$$

because the determinant of the product is the product of the determinants. Furthermore, if $k_i = k_j$ because the first and last region have the same potential, then the determinant is 1 (unimodular). This result is useful because $\mathbb{P}_i \mathbb{T}_i$ describes a system where the first and last region are identical so it is unimodular. It turns out a unimodular 2×2 matrix can be raised to an arbitrary power using

$$\mathbb{Q}^n = \mathbb{Q}U_{n-1}(q) - \mathbb{I}U_{n-2}(q), \quad (1.24)$$

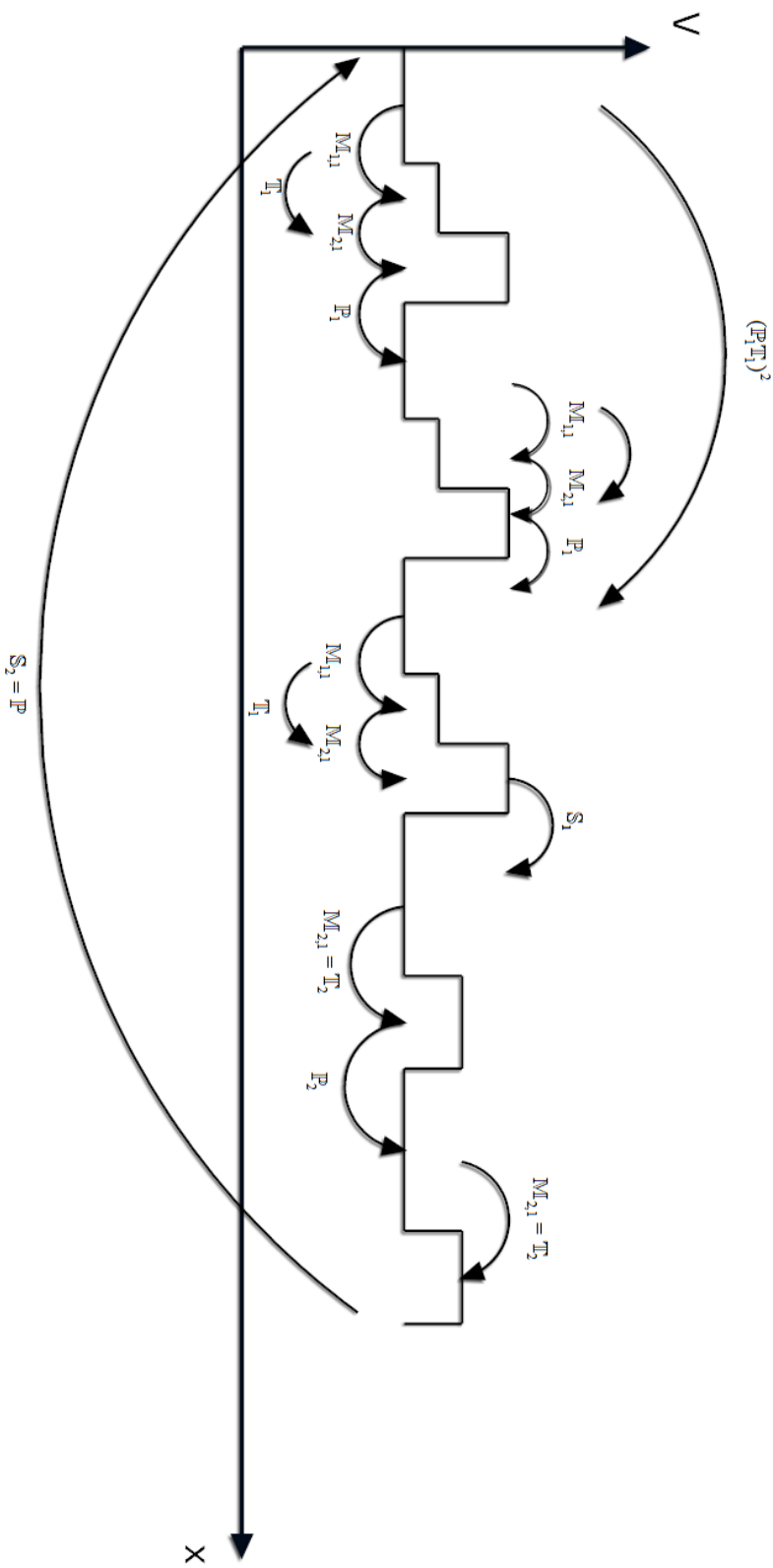


Figure 1.2: The purpose of this figure is to illustrate how Eq. 1.21 works. The system consists of two types of unit cells with three of the first kind and two of the second. The arrows represent how the various matrices shift coefficients. The $(\mathbb{T}_i)^{y_i-1}$ are responsible for moving the coefficients through a large number of unit cells quickly, and the S_i enforce continuity at the border between different unit cells.

where

$$U_n(q) = \frac{\sin [(n+1) \arccos(q)]}{\sqrt{1-q^2}} \quad (1.25)$$

are the Chebyshev polynomials of the second kind and

$$q \equiv \frac{1}{2} \text{Tr}(\mathbb{Q}). \quad (1.26)$$

The proof of this result is located in Appendix A.³ Because of these two results, evaluating Eq. 1.7 is reduced from as many matrix multiplications as there are regions to roughly as many as their are types of unit cells.

1.4.2 Properties of \mathbb{PT}

Another drawback of the method described in Sect. 1.3.2 is that it's not obvious the eigenvalues of \mathbb{PT} are degenerate at an allowed energy, meaning care must be taken when choosing which eigenvector is used to construct the wave function. This is overly complicated, though, because the eigenvalues are degenerate at an allowed energy. To prove this, consider that \mathbb{PT} at an allowed energy satisfies $\det(\mathbb{PT} - \mathbb{I}) = 0$ and is a transfer matrix so it has determinant one and is of the form[12]:

$$\begin{pmatrix} w & z \\ z^* & w^* \end{pmatrix}. \quad (1.27)$$

The square of the difference of the two eigenvalues of a 2×2 matrix, \mathbb{R} is

$$(\Delta\lambda)^2 = \text{Tr}(\mathbb{R})^2 - 4 \det(\mathbb{R}). \quad (1.28)$$

Taking $\mathbb{R} = \mathbb{PT}$, it's given that $\det(\mathbb{PT}) = 1$ because $\det(\mathbb{T}) = k_1/k_N$ and $\det(\mathbb{P}) = k_N/k_1$. Next, working with $\det(\mathbb{PT} - \mathbb{I}) = 0$:

$$\det(\mathbb{PT} - \mathbb{I}) = \begin{vmatrix} w - 1 & z \\ z^* & w^* - 1 \end{vmatrix} \quad (1.29)$$

$$= ww^* - zz^* - w - w^* + 1 \quad (1.30)$$

$$= \det(\mathbb{PT}) - \text{Tr}(\mathbb{PT}) + 1 \quad (1.31)$$

$$= 2 - \text{Tr}(\mathbb{PT}) = 0. \quad (1.32)$$

Which implies

$$\text{Tr}(\mathbb{PT}) = 2. \quad (1.33)$$

Therefore,

$$\Delta\lambda^2 = 0 \quad (1.34)$$

and the eigenvalues are degenerate.

This result means that rootfinding must be done on only one of the eigenvalues of \mathbb{PT} . However, there now seems to be an ambiguity in choosing which eigenvector to

³For an alternate derivation, see Griffiths and Steinke, 2001[12].

use to generate the wave function. The eigenvectors v_1 , and v_2 of Eq. 1.27 are given by:

$$\hat{v}_1 = \left(\frac{-2\sqrt{|z|^2 - \text{Im}(w)^2} - w^* + w}{2z^*}, 1 \right), \quad (1.35)$$

$$\hat{v}_2 = \left(\frac{2\sqrt{|z|^2 - \text{Im}(w)^2} - w^* + w}{2z^*}, 1 \right). \quad (1.36)$$

The term in the square root is just $\Delta\lambda$ which is zero at an allowed energy, so the eigenvectors are actually identical.

In this chapter we developed a method to solve for the energy eigenstates of an arbitrary piecewise constant potential. Heuristically, it works by selecting a system to be solved, and then solving an eigenvalue problem using rootfinding and then using a corresponding eigenvector to build the wave function. The method will solve the exact quantum dot model, and will also be used to solve the EMA and EFA.

Chapter 2

The Classic Solution

2.1 Introduction

This chapter will detail the two standard methods for finding the solutions to a one-dimensional quantum dot. The methods are called the envelope-function approximation (EFA) and effective-mass approximation (EMA). In outline, they work by solving the unperturbed lattice, solving an effective Schrödinger equation for the perturbing potential; the impurities that make a quantum dot, and then multiplying the two. The differences between the two methods will be discussed later. This chapter contains a derivation of Bloch's theorem, the Kronig-Penney model, the EFA, and the EMA. Also included is some basic solid state physics necessary for the derivation of the EFA and EMA.

2.2 Bloch's Theorem

Directly solving the Schrödinger equation for a periodic system is, in general, a Herculean task. Surprisingly, though, knowing that the potential is periodic does significantly restrict the solution space and provides just enough information to directly solve some simple systems. By periodic potential is meant a potential for which there exists an a , the period of the potential, such that for all x , $V(x + a) = V(x)$. The quantitative result is Bloch's Theorem.¹

Bloch's theorem states that given a periodic potential, the wave function has the property that

$$\psi(x - a) = e^{-ika}\psi(x), \quad (2.1)$$

where k is an index to label the solution and a is the period of the potential. What this means is that the wave function is periodic modulo a factor of magnitude one.

To prove this result, define an operator $\hat{T}(a)$ such that $\hat{T}(a)\psi(x) \equiv \psi(x - a)$. $\hat{T}(a)$ is called a translation operator because it translates the wave function in space. To

¹The proof presented here is based on lecture notes for Quantum Mechanics II, taught by Darrell Schroeter, Reed College, 2014.

determine $\hat{T}(a)$, consider the Taylor expansion of $\psi(x - a)$:

$$\psi(x - a) = \sum_{j=0}^{\infty} \frac{\psi^{(j)}(x)(-a)^n}{n!}. \quad (2.2)$$

Replacing derivatives with the momentum operator in the position basis, we can write:

$$\psi(x - a) = e^{-\frac{ia}{\hbar}\hat{p}}\psi(x) \quad (2.3)$$

, so

$$\hat{T}(a) = e^{-\frac{ia}{\hbar}\hat{p}}. \quad (2.4)$$

An essential property of $\hat{T}(a)$ is that it's unitary.

This proof of Bloch's Theorem also requires the result that the eigenvalues of a unitary operator have magnitude one. To see this, consider the following inner product where $|\alpha\rangle$ is an eigenstate of $\hat{T}(a)$ with eigenvalue a :

$$\langle \alpha | \hat{T}^\dagger(a)\hat{T}(a) | \alpha \rangle = \langle \alpha | \alpha \rangle \quad (2.5)$$

but,

$$\langle \alpha | \hat{T}^\dagger(a)\hat{T}(a) | \alpha \rangle = \langle \hat{T}(a)\alpha | \hat{T}(a)\alpha \rangle = aa^* \langle \alpha | \alpha \rangle \quad (2.6)$$

Hence, $aa^* = 1$, or, more usefully, $a = e^{ika}$ for some real k called the wave-vector because it has dimensions of inverse length and will turn out to have properties similar to its classical counterpart.

Next, consider the effect of the translation operator on the momentum and position operators. Also, assume that the translations are infinitesimal. Assuming infinitesimal translations doesn't change anything because a large translation can be built out of many infinitesimal ones. For position:

$$\hat{T}^\dagger(a)\hat{x}\hat{T}(a) = \left(1 + i\frac{\hat{p}}{\hbar}\right)\hat{x}\left(1 - i\frac{\hat{p}}{\hbar}\right), \quad (2.7)$$

$$= \hat{x} + i\frac{a}{\hbar}[\hat{p}, \hat{x}], \quad (2.8)$$

$$= \hat{x} + a. \quad (2.9)$$

For momentum, the only thing that changes is that the relevant commutator is $[\hat{p}, \hat{p}] = 0$, so

$$\hat{T}^\dagger(a)\hat{p}\hat{T}(a) = \hat{p}. \quad (2.10)$$

Now, consider a Hamiltonian with a periodic potential so that $V(\hat{x}+a) = V(\hat{x})$ where a is the period of the potential. Transforming the Hamiltonian with a translation of a returns:

$$\hat{T}^\dagger(a)\hat{H}(\hat{x}, \hat{p})\hat{T}(a) = \hat{H}(\hat{x} + a, \hat{p}) \quad (2.11)$$

$$= \frac{\hat{p}^2}{2m} + V(\hat{x} + a) \quad (2.12)$$

$$= \frac{\hat{p}^2}{2m} + V(\hat{x}). \quad (2.13)$$

Hence,

$$\hat{T}^\dagger(a)\hat{H}\hat{T}(a) = \hat{H}. \quad (2.14)$$

Multiplying both sides by a $\hat{T}(a)$ and subtracting leads to:

$$[\hat{H}, \hat{T}(a)] = 0. \quad (2.15)$$

The commutator vanishing means that there exist simultaneous eigenstates of both \hat{H} and $\hat{T}(a)$.² Consider such a wave function, $\psi(x)$, then:

$$\hat{T}(a)\psi(x) = \psi(x - a) = e^{-ika}\psi(x). \quad (2.16)$$

Thus completing the proof.

This form of the theorem is sufficient for deriving the Kronig-Penney model, but it will be needed in a different form for deriving the envelope-function approximation. To derive the alternate form, ansatz that $\psi_{n,k}(x) = e^{ikx}u_{n,k}(x)$ where nothing is known about u and n, k label the u to enforce that they're not necessarily identical. Plugging this into Eq. 2.16 returns $u_{n,k}(x - a) = u_{n,k}(x)$. This means that

$$\psi_{n,k}(x) = e^{ikx}u_{n,k}(x) \quad (2.17)$$

where u is some function that has the same periodicity as the lattice.

2.3 Useful Concepts from Solid State Physics

Section. 2.5 contains a derivation of the envelope-function approximation and requires two concepts that may not be familiar to students that have not studied solid state physics. The first is quasi-momentum and the second is effective mass.³

2.3.1 Quasi-Momentum

The purpose of this sub-section is to derive an equation for the time evolution of a state that satisfies Bloch's theorem under the influence of a constant force, F so the Hamiltonian becomes $\hat{H} = \hat{H}_0 - F\hat{x}$. As a consequence, we will find a new definition for the momentum of a particle. To do so, we calculate

$$\frac{d\langle n, k | \hat{T}(a) | n, k \rangle}{dt} \quad (2.18)$$

where $|n, k\rangle$ satisfies Bloch's theorem. Performing the calculation:

$$\frac{d\langle n, k | \hat{T}(a) | n, k \rangle}{dt} = -e^{-ika}ia\frac{dk}{dt}. \quad (2.19)$$

²For a proof of this, see Sakurai's *Modern Quantum Mechanics*, Section 1.4[14].

³Both my exposition of quasi-momentum and effective mass come from Kittel, *Introduction to Solid State Physics*[1].

By the Ehrenfest theorem,

$$\frac{d\langle \hat{T}(a) \rangle}{dt} = \frac{i}{\hbar} \left\langle [\hat{H}, \hat{T}(a)] \right\rangle. \quad (2.20)$$

Calculating the right-hand side

$$\left\langle [\hat{H}, \hat{T}(a)] \right\rangle = F \left\langle [\hat{T}(a), \hat{x}] \right\rangle \quad (2.21)$$

$$= F \langle n, k | \hat{T}(a) \hat{x} - \hat{x} \hat{T}(a) | n, k \rangle \quad (2.22)$$

$$= F \langle n, k | \hat{T}(a) \hat{x} \hat{T}(a)^\dagger \hat{T}(a) - \hat{x} \hat{T}(a)^\dagger \hat{T}(a) | n, k \rangle \quad (2.23)$$

$$= F \langle n, k | (\hat{x} - a) \hat{T}(a) - \hat{x} \hat{T}(a) | n, k \rangle \quad (2.24)$$

$$= -F \langle n, k | a \hat{T}(a) | n, k \rangle \quad (2.25)$$

$$= -a F e^{-ika}. \quad (2.26)$$

Hence, by Eq. 2.20,

$$\hbar \frac{dk}{dt} = F. \quad (2.27)$$

This last equation looks very similar to Newton's second law, which suggests we make the identification

$$p = \hbar k. \quad (2.28)$$

What has happened is that we've figured out how a wave-packet evolves in time under the influence of constant force.⁴ We will use this momentum to perform a Fourier transform in the derivation of the EFA.

2.3.2 Effective Mass

The second tool needed to derive the EFA is the idea of effective mass. To see how it arises, first consider the definition for the group velocity of a wave packet:

$$v_g \equiv \frac{1}{\hbar} \frac{dE_n(k)}{dk}, \quad (2.29)$$

where $E_n(k)$ is the energy that would come from solving for the eigenvalues of the periodic potential. We differentiate Eq. 2.29 to get

$$\frac{dv_g}{dt} = \frac{1}{\hbar} \frac{d^2E_n(k)}{dkdt} \quad (2.30)$$

$$= \frac{1}{\hbar} \frac{d^2E_n(k)}{dk^2} \frac{dk}{dt}. \quad (2.31)$$

Using Eq. 2.27, this becomes

$$F = \hbar^2 \left(\frac{d^2E_n(k)}{dk^2} \right)^{-1} \frac{dv_g}{dt}. \quad (2.32)$$

⁴This derivation is hardly rigorous because it's never shown $dk/dt \neq 0$. For a rigorous, but very technical, derivation, see J. Zak, 1967 [15]

This last equation is also recognizable as a version of Newton's second law if we define the effective mass to be

$$m^* \equiv \hbar^2 \left(\frac{d^2 E_n(k)}{dk^2} \right)^{-1}. \quad (2.33)$$

The effective mass allows us to calculate how the group velocity of an electron wavepacket changes under the influence of a constant external force. Note that the actual mass of an electron doesn't change, but what has happened is that we've found a way to account for all the influence of the lattice on the electron by simply adjusting the value of its mass. In fact it can be directly measured by determining the cyclotron frequency of electrons in a material[1].

With these results we can write a Taylor series for the energy of an electron assuming the dispersion relation is symmetric and mostly parabolic around some wavevector k_0 . This series is

$$E_n(k_0 + \delta k) \approx E_n(k_0) + \frac{\delta k^2}{2} \left. \frac{d^2 E_n(k)}{dk^2} \right|_{k=k_0} \quad (2.34)$$

$$= E_n(k_0) + \frac{(\delta k \hbar)^2}{2m^*} \quad (2.35)$$

$$= E_n(k_0) + \frac{p^2}{2m^*} \quad (2.36)$$

This equation is deceptively simple because m^* depends on k in some complicated way, but it is essential for finishing the derivation of the EFA.

2.4 The Kronig-Penney Model

The unperturbed lattice of the quantum dot model is known at the Kronig-Penney model. Using Bloch's theorem, it's possible to solve for the energies of the model. To do this, consider one unit cell of the lattice, just the first two regions of the potential shown in Fig. 4, a region of length a and potential $V = 0$ adjacent to a region of length b and potential $V = U_0$. Using the definitions of the previous chapter, continuity of the wave function and its derivative between the two regions can be expressed as

$$\begin{pmatrix} A_2 \\ B_2 \end{pmatrix} = \mathbb{M}_1 \begin{pmatrix} A_1 \\ B_1 \end{pmatrix}. \quad (2.37)$$

The next step is to use Bloch's Theorem to impose boundary conditions. By Bloch's Theorem,

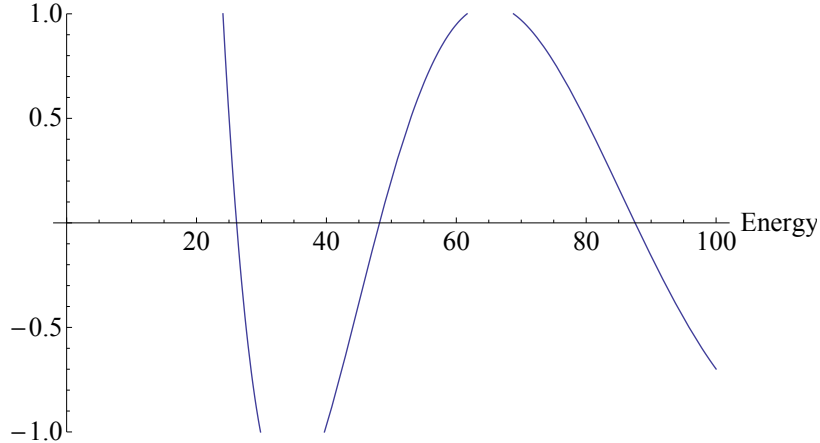
$$\psi(a + b) = e^{ik(a+b)} \psi(0) \quad (2.38)$$

$$\psi'(a + b) = e^{ik(a+b)} \psi'(0). \quad (2.39)$$

The first condition can be written as

$$e^{ik(a+b)} (A_1 + B_1) = e^{ik_2 b} A_2 + e^{-ik_2 b} B_2 \quad (2.40)$$

Figure 2.1: The last two terms of Eq. 2.45. Where the magnitude of the function exceeds one, a real k does not exist. The regions where k does exist are called bands and the regions where it doesn't are bandgaps.



and the second

$$e^{ik(a+b)}(ik_1 A_1 - ik_1 B_1) = e^{ik_2 b} ik_2 A_2 - e^{-ik_2 b} ik_2 B_2. \quad (2.41)$$

we combine these into a matrix-vector expression:

$$\begin{pmatrix} e^{ik(a+b)} & e^{ik(a+b)} \\ e^{ik(a+b)} ik_1 & -e^{ik(a+b)} ik_1 \end{pmatrix} \begin{pmatrix} A_1 \\ B_1 \end{pmatrix} = \begin{pmatrix} e^{ik_2 b} & e^{-ik_2 b} \\ e^{ik_2 b} ik_2 & -e^{-ik_2 b} ik_2 \end{pmatrix} \begin{pmatrix} A_2 \\ B_2 \end{pmatrix}, \quad (2.42)$$

$$\begin{pmatrix} e^{ik(a+b)} & e^{ik(a+b)} \\ e^{ik(a+b)} ik_1 & -e^{ik(a+b)} ik_1 \end{pmatrix} \begin{pmatrix} A_1 \\ B_1 \end{pmatrix} = \begin{pmatrix} e^{ik_2 b} & e^{-ik_2 b} \\ e^{ik_2 b} ik_2 & -e^{-ik_2 b} ik_2 \end{pmatrix} \mathbb{M}_1 \begin{pmatrix} A_1 \\ B_1 \end{pmatrix}, \quad (2.43)$$

$$\begin{pmatrix} A_1 \\ B_1 \end{pmatrix} = \begin{pmatrix} e^{ik(a+b)} & e^{ik(a+b)} \\ e^{ik(a+b)} ik_1 & -e^{ik(a+b)} ik_1 \end{pmatrix}^{-1} \begin{pmatrix} e^{ik_2 b} & e^{-ik_2 b} \\ e^{ik_2 b} ik_2 & -e^{-ik_2 b} ik_2 \end{pmatrix} \mathbb{M}_1 \begin{pmatrix} A_1 \\ B_1 \end{pmatrix}. \quad (2.44)$$

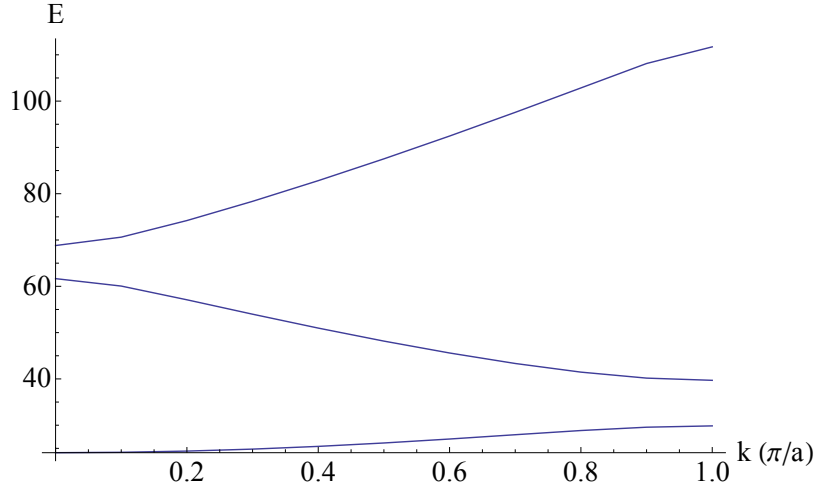
Eq. 2.44 is recognizable as another eigenvalue problem. Handling the eigenvalue problem in the same manner as in the previous chapter, and after considerable simplification, we obtain the following transcendental, implicit, equation for the allowed energies:

$$0 = \cos[ak_1] \cos[bk_2] - \frac{k_1^2 + k_2^2}{2k_1 k_2} \sin[ak_1] \sin[bk_2] - \cos[k(a+b)]. \quad (2.45)$$

One interesting property of this result is that the magnitude of the first two terms is not bounded by 1. The unboundedness means that there can be energies such that a real k does not exist, in violation of Bloch's theorem. To see what this nonexistence means graphically, see Fig. 2.1 and Fig. 2.2. Fig. 2.1 is an example plot of the first two terms of Eq. 2.45 and Fig. 2.2 is an example dispersion relation. The point is that there are large, continuous sets of energy for which k does not exist. These regions are forbidden, and their width is the value of a bandgap.

The standard derivation of this model uses a 4×4 determinant problem to obtain Eq. 2.45[1]. One advantage of the above derivation, besides maintaining continuity

Figure 2.2: The solutions to Eq. 2.45 plotted as a dispersion relation. The most important feature of this plot is that the bandgaps alternate between occurring at $k = 0$ and $k = \pi/a$.



with the methods described in the previous chapter, is that it makes it clear how to construct the wave function by choosing A_1, B_1 to be an eigenvector of the matrix in 2.44.

It also turns out, that for appropriate choices of k , the methods of the previous chapter can be used to solve for energies and wave functions. To demonstrate this, let L be the length of the region on which periodic boundary conditions are imposed and $L = Na$ where N is the number of unit cells and a is the lattice constant. In this case, Bloch's Theorem states

$$\psi(L) = e^{ikNa} \psi(0). \quad (2.46)$$

Which reduces to periodic boundary conditions when

$$kNa = 2\pi m, \quad (2.47)$$

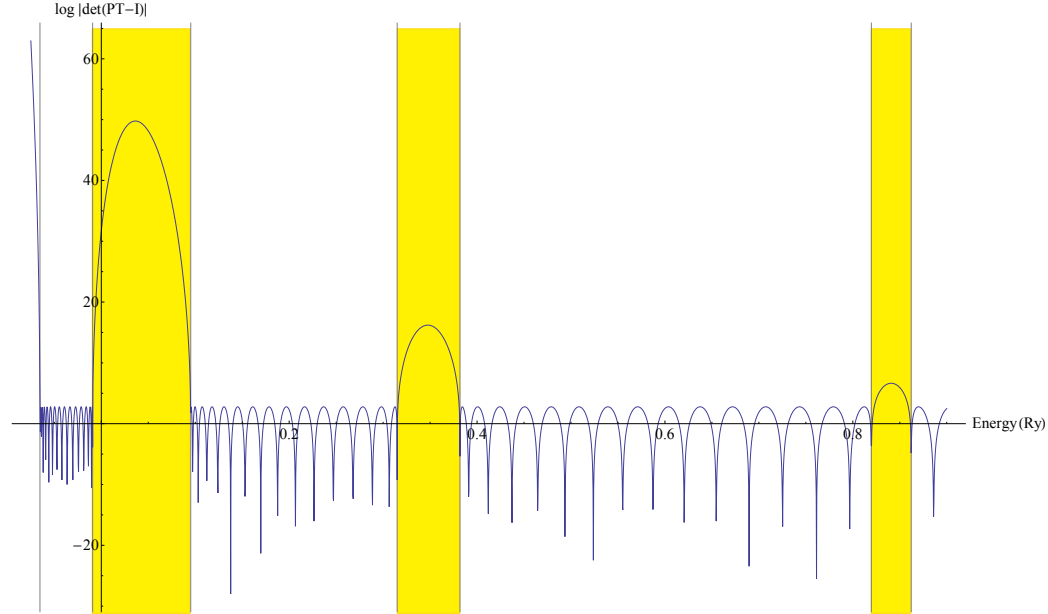
where m is an integer. Rearranging Eq. 2.47 means allowed values of k are given by

$$k = \frac{2\pi m}{Na}, \quad (2.48)$$

which is just the standard definition for the allowed wavevectors of a particle in a periodic box. Therefore, as long as k is chosen according to Eq. 2.48, the Kronig-Penney model is solvable using the methods developed in the previous chapter which means that wave functions can be easily constructed.

To label a solution to this model, it's insufficient to use only k because in general there will be more than one solution for any given k . To fix this, we add a second label, n , called the band index to specify which band the k is partnered with. k and n are sufficient to label a solution not only for the Kronig-Penney model, but for any solution to a periodic potential; even in higher dimensions with the caveat that k becomes a vector. Therefore, solutions to periodic potentials will, for the rest of the thesis, be labeled as $|n, k\rangle$, or simple variations thereof.

Figure 2.3: The exact method and Kronig-Penney agree on the band edges of a series of square wells. The yellow shaded regions are bandgaps and the downward spikes represent allowed states. Also, because the exact method doesn't have a wave vector argument, it finds all allowed states.



2.4.1 Method Validation

We can use Kronig-Penney to show the exact method we've developed actually works. To do so, we simply found the band edges for a Kronig-Penney model, plotted $\det(\mathbb{P}\mathbb{T} - \mathbb{I})$, and superimposed the two. The agreement is demonstrated in Fig. 2.3.

2.5 The Envelope-Function Approximation

The next step in the classic solution is determining how a perturbation to the lattice affects the energies and wave functions of an electron in a region of high-symmetry in the dispersion relation. The standard method for doing this is called the envelope-function approximation.⁵

To start, write the Schrödinger equation as:

$$[\hat{H}_0 + \hat{V}] |\psi\rangle = E |\psi\rangle \quad (2.49)$$

where \hat{H}_0 is the Hamiltonian of the unperturbed lattice and has known solutions, and $\hat{V}(x)$ is the perturbation. The perturbation is assumed to be both small and

⁵This derivation follows Springer, Appendix A[9].

slowly varying on the scale of the lattice constant. The eigenstates of \hat{H}_0 , $|n, k\rangle$, with eigenvalue $E_n(k)$, form a complete basis so we can write

$$|\psi\rangle = \sum_{n,k} |n, k\rangle \langle n, k| \psi \rangle . \quad (2.50)$$

Substituting Eq. 2.50 into Eq. 2.49 yields

$$\sum_{n',k'} E'_n(k) |n', k'\rangle \langle n', k'| \psi \rangle + \hat{V} \sum_{n',k'} |n', k'\rangle \langle n', k'| \psi \rangle = E \sum_{n',k'} |n', k'\rangle \langle n', k'| \psi \rangle . \quad (2.51)$$

We then take the inner product of this equation with $\langle n, k|$ and exploit the orthonormality of the eigenstates to find

$$E_n(k) \langle n, k| \psi \rangle + \sum_{n',k'} \langle n, k| \hat{V} |n', k'\rangle \langle n', k'| \psi \rangle = E \langle n, k| \psi \rangle . \quad (2.52)$$

At this point, the goal is to determine the matrix values of \hat{V} by using simplifying approximations. In order to use the assumption that the potential is slowly varying, we must first evaluate the Fourier series of V :

$$\hat{V} = \sum_K e^{iKx} V_K \quad (2.53)$$

where

$$V_K = \frac{1}{L} \int e^{-iKx} \hat{V}(x) dx \quad (2.54)$$

and L is the length of the system. Inserting this into the matrix element of \hat{V} :

$$\langle n, k| \hat{V} |n', k'\rangle = \sum_K V_K \langle n, k| e^{iKx} |n', k'\rangle . \quad (2.55)$$

By assuming that the perturbation is slowly varying relative to the underlying lattice, V_K is only appreciable when $Ka \ll \pi$. We can also use the periodicity of the lattice to establish a relationship between k , k' , and K . Consider that

$$\langle n, k| V |n', k'\rangle = \sum_K V_K \langle n, k| e^{iKx} |n', k'\rangle \quad (2.56)$$

$$= \sum_K V_K \langle n, k| \hat{T}(a) \hat{T}(a)^\dagger e^{iKx} \hat{T}(a) \hat{T}(a)^\dagger |n', k'\rangle \quad (2.57)$$

$$= \sum_K V_K \langle \hat{T}(a)^\dagger n, k| \hat{T}(a)^\dagger e^{iKx} \hat{T}(a) | \hat{T}(a)^\dagger n', k'\rangle \quad (2.58)$$

$$= \sum_K V_K e^{ia(-k+K+k')} \langle n, k| e^{iKx} |n', k'\rangle \quad (2.59)$$

For this to be true, it must be the case that

$$e^{ia(-k+K+k')} = 1 \quad (2.60)$$

or,

$$\langle n, k | V | n', k' \rangle = 0. \quad (2.61)$$

The latter case is not interesting because it means the perturbation doesn't affect the system, so we choose the former which implies

$$a(-k + K + k') = 2\pi n \quad (2.62)$$

for some integer n . This last equation is identical to the definition of a reciprocal lattice vector, so we've learned that

$$-k + K + k' = G, \quad (2.63)$$

where G is a reciprocal lattice vector. We now make use of the assumptions that the potential is slowly varying and that the electron is near a zone center. If we write Eq. 2.63 in terms of its allowed values, we get

$$\frac{-2\pi j}{L} + \frac{2\pi l}{L} + \frac{2\pi m}{L} = \frac{2\pi nN}{L} \quad (2.64)$$

$$-j + l + m = nN \quad (2.65)$$

for integers j, l, m, n and where N is the number of unit cells. By assumption, j, l, m are all small compared to N , so this equation only has a solution when $n = 0$, so $G = 0$. Hence,

$$k' = k - K. \quad (2.66)$$

We are now ready to evaluate the matrix elements of \hat{V} . First, we define the position representation of $|n, k\rangle$ as $\phi_{n,k}(x)$. Evaluating the elements:

$$\langle n, k | V | n', k' \rangle = \sum_K V_K \langle n, k | e^{iKx} | n', k' \rangle \quad (2.67)$$

$$= \sum_K V_K \langle n, k | e^{iKx} | n', k - K \rangle \quad (2.68)$$

$$= \sum_K V_K \int \phi_{n,k}^*(x) e^{iKx} \phi_{n',k-K}(x) dx \quad (2.69)$$

$$= \sum_K V_K \int u_{n,k}^*(x) e^{-ikx} e^{iKx} e^{i(k-K)x} u_{n',k-K}(x) dx \quad (2.70)$$

$$= \sum_K V_K \int u_{n,k}^*(x) u_{n',k-K}(x) dx. \quad (2.71)$$

Remembering that K is small and assuming that the $u_{n,k}(x)$ do not change quickly with k , then we have

$$\int u_{n,k}^*(x) u_{n',k-K}(x) dx \approx \delta_{n,n'}. \quad (2.72)$$

At this point it's worth noting that the approximation has eliminated inter-band coupling with the $\delta_{n,n'}$. Inserting this into Eq. 2.52, we arrive at the principal result of the envelope-function approximation:

$$E_n(k) \langle n, k | \psi \rangle + \sum_K V_K \langle n, k - K | \psi \rangle = E \langle n, k | \psi \rangle. \quad (2.73)$$

This is technically a solution, but it is an equation in momentum space while we're accustomed to working in position space. Normally, to convert it to position space, an inverse Fourier transform is performed, but because the momenta are discreet, $p = \hbar k$, we instead use a Fourier series:

$$\sum_k E_n(k) e^{ikx} \langle n, k | \psi \rangle + \sum_k \sum_K e^{ikx} V_K \langle n, k - K | \psi \rangle = E \sum_k e^{ikx} \langle n, k | \psi \rangle. \quad (2.74)$$

The quantity $\sum_k e^{ikx} \langle n, k | \psi \rangle$ is defined to be the envelope-function, $F_n(x)$. Each of these terms can be further simplified. To simplify the first term, because we're working in an area of high symmetry, $E_n(k)$ can be replaced by Eq. 2.36. So the first term can be re-written as

$$\sum_k \left(E_n(k) + \frac{(\hbar k)^2}{2m^*} \right) e^{ikx} \langle n, k | \psi \rangle. \quad (2.75)$$

The momentum, because it's now acting on a state in position representation, can be converted to derivatives and pulled out of the sum, leaving

$$\left(E_n(k_0) - \frac{\hbar^2}{2m^*} \frac{d^2}{dx^2} \right) \sum_k e^{ikx} \langle n, k | \psi \rangle = \left(E_n(k) - \frac{\hbar^2}{2m^*} \frac{d^2}{dx^2} \right) F_n(x). \quad (2.76)$$

For the second term, we pull

$$V_K e^{iKx} \quad (2.77)$$

through the sum on k which turns the term into

$$\sum_k \sum_K e^{ikx} V_K \langle n, k - K | \psi \rangle = \sum_k V_K e^{iKx} \sum_K e^{i(k-K)x} \langle n, k - K | \psi \rangle \quad (2.78)$$

$$= V(x) F_n(x). \quad (2.79)$$

The final term is simply

$$E F_n(x). \quad (2.80)$$

Putting it all together we obtain the following equation to solve for the envelope-function

$$\left(E_n(k) - \frac{\hbar^2}{2m^*} \frac{d^2}{dx^2} + V(x) \right) F_n(x) = E F_n(x). \quad (2.81)$$

2.81 is recognizable as a Schrödinger equation. It can be simplified by omitting the $E_n(k)$ because additive constants to Hamiltonians don't affect the physics, yielding

$$\left(-\frac{\hbar^2}{2m^*} \frac{d^2}{dx^2} + V(x) \right) F_n(x) = \epsilon F_n(x) \quad (2.82)$$

which is simpler and the total energy is just

$$E = \epsilon + E_n(k). \quad (2.83)$$

Having the Schrödinger equation as a result is excellent because we know how to solve it using the results of Chapter 1, but what's not obvious is how this helps us find the wave functions. To see its relevance, consider the original expansion of the wave function in terms of solutions to the unperturbed system:

$$|\psi\rangle = \sum_k |n, k\rangle \langle n, k| \psi \rangle \quad (2.84)$$

and we no longer sum over l because we know interband terms vanish. $|n, k\rangle$ satisfies Bloch's theorem, so Eq. 2.84 can be written as

$$\psi(x) = \sum_k \langle n, k | \psi \rangle e^{ikx} u_{n,k}(x). \quad (2.85)$$

If we assume that $u_{n,k}(x)$ doesn't change quickly with k , then we can factor it out of the sum and set $k \rightarrow k_0$ where k_0 is the symmetry point of the dispersion relation. This assumption allows us to simplify the expression to:

$$\sum_k \langle n, k | \psi \rangle e^{ikx} u_{n,k}(x) = u_{n,k_0}(x) \sum_k e^{ikx} \langle n, k | \psi \rangle, \quad (2.86)$$

$$= \phi_{n,k_0}(x) e^{-ik_0 x} \sum_k e^{ikx} \langle n, k | \psi \rangle, \quad (2.87)$$

$$= \phi_{n,k_0}(x) e^{-ik_0 x} F_n(x). \quad (2.88)$$

If we choose $k_0 = 0$, we have the simple result that

$$\psi(x) = \phi_{n,0}(x) F_n(x). \quad (2.89)$$

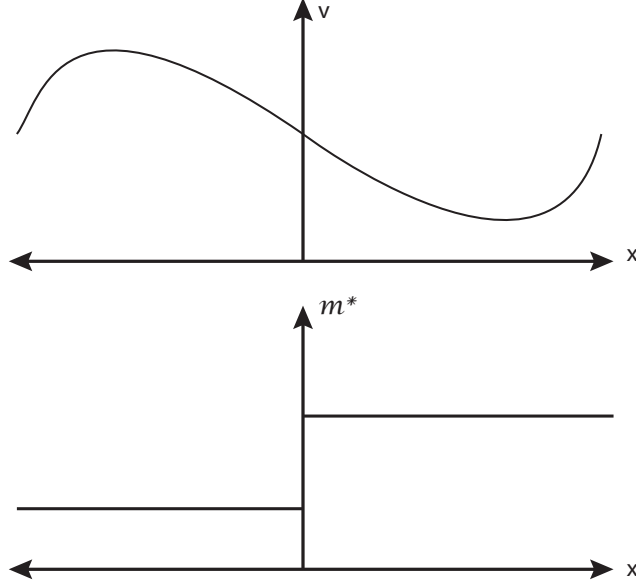
2.6 The Effective-Mass Approximation

The effective-mass approximation (EMA) is a sibling approximation to the EFA. The EMA is a heuristic as opposed to the procedural EFA. The central idea of the EMA is to instead model the system as the junction of bulk materials[11]. Because the materials are assumed to be bulk, each material has a well-defined effective mass. Therefore, we can write as a new effective Schrödinger for the envelope-function

$$\frac{-\hbar^2}{2} \frac{d}{dx} \left(\frac{1}{m^*(x)} \frac{dF_n(x)}{dx} \right) + V(x) F_n(x) = \epsilon F_n(x) \quad (2.90)$$

where the effective mass is now position dependent and the new form of the kinetic term is required to preserve Hermiticity[11]. Treating the system as the junction of two bulk materials has the effect of allowing us to simplify $V(x)$ because the effects of the different lattice constants are now contained in $m^*(x)$; $V(x)$ is just the average

Figure 2.4: Example potential used for deriving envelope-function boundary conditions for the effective-mass approximation.



perturbation, U_p for the quantum dot model. If we assume that the wave function is similar in these two bulk materials, then we still have

$$\psi(x) = \phi_{n,0}(x)F_n(x) \quad (2.91)$$

where $\phi_{n,0}(x)$ is chosen to be the wave function of the dominant material.

One interesting property of this approximation is that it requires new boundary conditions for $F_n(x)$ at the junction of two regions with different effective masses. The condition that $F_n(x)$ be continuous is still valid, but the boundary conditions for the derivative must be modified. To derive this new boundary condition, consider a system where the effective mass is discontinuous at 0. Such a system is shown in Fig. 2.4. Next, we integrate Eq. 2.90 over the discontinuity:

$$\frac{-\hbar^2}{2} \int_{-\delta}^{\delta} \frac{d}{dx} \left(\frac{1}{m^*(x)} \frac{dF_n(x)}{dx} \right) dx + \int_{-\delta}^{\delta} V(x)F_n(x)dx = \epsilon \int_{-\delta}^{\delta} F_n(x)dx. \quad (2.92)$$

We then take the limit as $\delta \rightarrow 0$ which eliminates the second two terms and we are left with

$$\frac{1}{m^*(\delta)} \frac{dF_n(\delta)}{dx} = \frac{1}{m^*(-\delta)} \frac{dF_n(-\delta)}{dx}. \quad (2.93)$$

There are two interesting consequences of Eq. 2.93. First, the wave function predicted has a kink, which is strictly speaking unphysical because the potential capable of kinking a wave function is a Dirac delta, which do not exist. Secondly, the methods of Chapter 1 don't directly apply to solving this problem because those

methods assume $F'(x)$ is continuous. The lack of direct applicability is overcome by simply re-deriving Eq. 1.5 with the appropriate continuity conditions. Doing so yields

$$\mathbb{M}_i = \frac{1}{2} \begin{pmatrix} e^{il_i k_i} (1 + \beta_i) & e^{-il_i k_i} (1 - \beta_i) \\ e^{il_i k_i} (1 - \beta_i) & e^{-il_i k_i} (1 + \beta_i) \end{pmatrix}, \quad (2.94)$$

where

$$\beta_i \equiv \frac{m_{i+1}^* k_i}{m_i^* k_{i+1}}, \quad (2.95)$$

and k_i is now

$$k_i = \frac{\sqrt{2m_i^*(E - V_i)}}{\hbar}. \quad (2.96)$$

The determinants of the these new matrices are β_i , so \mathbb{PT} will still be unimodular because the same cancellations will still take place. By knowing the form of the new matrices and that their determinant still has the form of a simple ratio, we can now proceed using the formalism developed in Chapter 2 to find energies and wave functions. For verification, note Eq. 2.94 reduces to Eq. 1.5 if $m_i^* = m_{i+1}^*$.

Chapter 3

Results

In this chapter we first describe how the methods outlined in Chapters 2 and 3 are applied to the model of the quantum dot, including the relevant numerics. A particular model to be solved is then constructed, solved, and the results are compared.

3.1 Applying Solution Methods

3.1.1 Exact Method

In the case of the exact method, we first need to figure out the form of Eq. 1.21. To do this, we just insert the potential defined in Eq. 4 into Eq. 1.21. Doing so yields

$$\mathbb{PT} = \mathbb{PM}_{1,2} (\mathbb{P}_2 \mathbb{M}_{1,2})^{\lfloor N_0 - \gamma N_p - 1 \rfloor} \mathbb{S}_2 \mathbb{S}_1 \mathbb{M}_{1,1} (\mathbb{P}_1 \mathbb{M}_{1,1})^{N_p - 1}. \quad (3.1)$$

This equation isn't obvious, so a diagrammatic version of its derivation is shown in Fig. 3.1.

The next question is how to find the roots of $r(E) = \det(\mathbb{PT} - \mathbb{I})$. The first problem is that $r(E)$ is generally complex. This is solved by instead rootfinding on $|r(E)|$. This means that regular bisection is no longer available as a rootfinding method because $|r(E)|$ is never negative, but what we can do is rootfinding on the derivative. However, this will return all extrema of the function, not just the zeros and there is also the question of calculating the derivative.

While *Mathematica* could symbolically calculate the exact derivative of Eq. 3.1 for a given energy, this is extremely slow and instead we must use a numerical derivative. To derive an approximation for $f'(x)$, we consider the Taylor approximations for $f(x_0 + \Delta x)$ and $f(x_0 - \Delta x)$:¹

$$f(x_0 + \Delta x) \approx f(x_0) + \Delta x f'(x_0) \quad (3.2)$$

$$f(x_0 - \Delta x) \approx f(x_0) - \Delta x f'(x_0). \quad (3.3)$$

¹The derivation for the numerical derivatives come from Joel Franklin's *Computational Methods for Physics*[16].

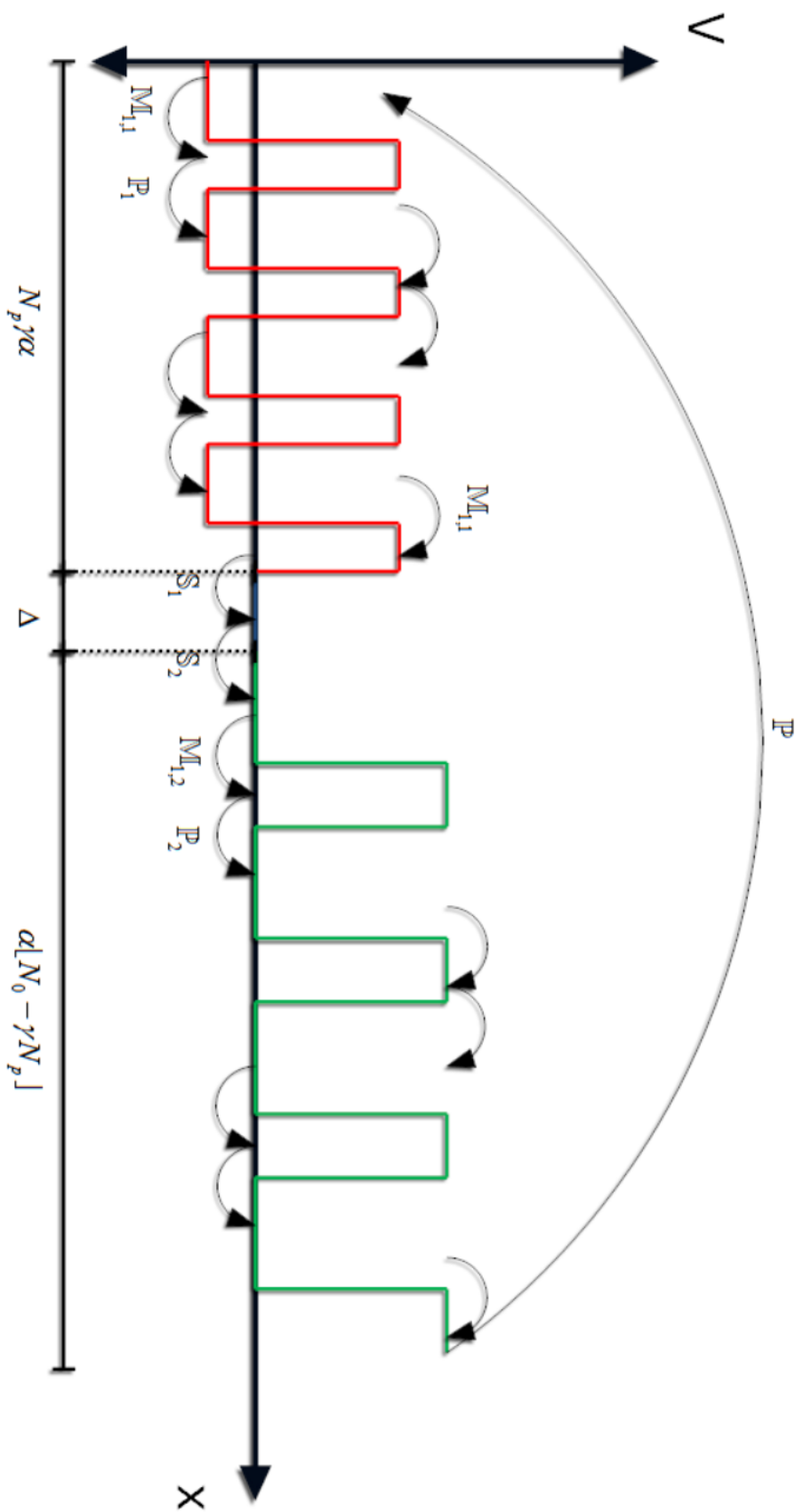
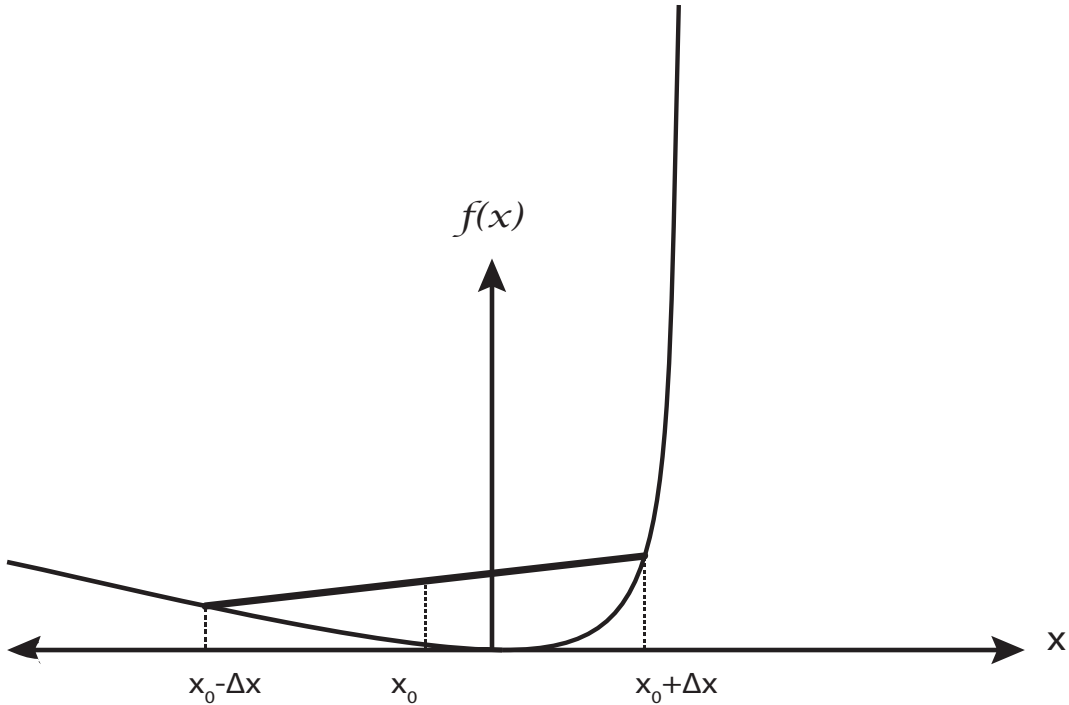


Figure 3.1: This graphical derivation of \mathbb{PT} for the exact potential is analogous to Fig. 1.2.

Figure 3.2: Demonstration that it's possible to miscalculate the sign of the derivative which can cause the bisection routine to converge to a value outside the error tolerance of the actual root.



Subtracting these and re-arranging yields

$$f'(x_0) \approx \frac{f(x_0 + \Delta x) - f(x_0 - \Delta x)}{2\Delta x}. \quad (3.4)$$

With this equation for the derivative and bisection we can now find the extrema of $|r(E)|$. One oddity of this method is that $2\Delta x$ must be smaller than the target accuracy of the bisection routine. This requirement is demonstrated in Fig. 3.2.

As for the issue of this picking out all extrema of the function, we don't worry about this because the functions we're trying to find the roots of have sufficiently few extrema that we can just go through the proposed roots by hand. While slow, it's reliable and works.

3.1.2 Envelope-Function Approximation

There are three main steps in applying the envelope-function approximation. First, a solution to the Kronig-Penney model must be found. Second, we need the effective mass corresponding to that solution. Finally, we need to solve the effective Schrödinger equation, Eq. 2.82.

Solving the Kronig-Penney model involves finding the roots of Eq. 2.45 for a given k . It turns out that this equation is real, so simple bisection can be used. The only issue is that if we are looking for a solution to a higher band, we need to find as many roots as the desired band index. This is fairly simple to accomplish; you simply restart bisection after each root.

Once a solution has been found the next problem is calculating an effective mass. To do this, we use Eq. 2.33 and approximate the derivative using numerics. The numerical second derivative we use for a function $f(x)$ can be derived by considering its Taylor expansion out to second order:

$$f(x_0 + \Delta x) \approx f(x_0) + \Delta x f'(x_0) + \frac{\Delta x^2}{2} f''(x_0) \quad (3.5)$$

$$f(x_0 - \Delta x) \approx f(x_0) - \Delta x f'(x_0) + \frac{\Delta x^2}{2} f''(x_0), \quad (3.6)$$

adding these and rearranging yields

$$f''(x_0) \approx \frac{f(x_0 - \Delta x) - 2f(x_0) + f(x_0 + \Delta x)}{\Delta x^2}. \quad (3.7)$$

This approximation for second derivatives along with bisection allow the calculation of effective masses. Finally, we need to calculate the solutions to Eq. 2.82. To find the relevant potential we use the algorithm for subtracting potentials described in the Introduction and then use the method of the exact solution to find its solutions. Unfortunately, because the form of the potential for the EFA doesn't have a closed form expression, we can't explicitly construct something like Eq. 3.1, so we have to use Eq. 1.7 to calculate PT . It may be possible to write a program that creates an equation analogous to Eq. 3.1, but that would require machine recognition of useful patterns, which is beyond the scope of this work.

3.2 Effective-Mass Approximation

The first steps of applying the EMA are identical to solving the EFA; we solve Kronig-Penney and determine the relevant effective mass. Where it diverges is in the solution of the effective Schrödinger equation. The solution diverges because the potential is not directly derivable from the others, and we must use the more general \mathbb{M}_i defined in Eq. 2.94. We take the potential to be a finite square well whose depth is simply U_p , Δ is counted as part of the unperturbed lattice, and the effective mass is a step function. The perturbation is shown in Fig. 8. The step function effective mass means the effective mass must be computed twice; once for the unperturbed lattice and once for the perturbed lattice. Because the potential is relatively simple, we can derive the following equation for the energies by using the results of Chapter 2 and Eq. 2.94:

$$-1 = \frac{(k_2 m_1^* - k_1 m_2^*)^2 \cos[l(k_1 + k_2) - k_2 L] - (k_2 m_1^* + k_1 m_2^*)^2 \cos[l(k_1 - k_2) + k_2 L]}{4k_1 k_2 m_1^* m_2^*}, \quad (3.8)$$

where $l = \alpha\gamma N_p$, $L = \alpha N_0$, m_1^* is the effective mass in the perturbed lattice, and m_2^* is the effective mass in the unperturbed lattice. This equation generally returns complex values, so rootfinding is done on its magnitude.

3.3 Building the Model

Although the purpose of this thesis is to evaluate the validity of the EFA and EMA, and therefore doesn't strictly speaking need to be physical, we still choose to construct a somewhat physical model to ground the results. First, we will describe the choice of units, then how we pick the parameters of the Kronig-Penney lattice, and, finally, how we choose perturbation parameters.

3.3.1 Units

To non-dimesionalize the problem, we set the energy and length scale using

$$x = a_0 \tilde{x} \quad E = \text{Ry} \tilde{E} \quad V(x) = \text{Ry} \tilde{V}(x) \quad (3.9)$$

where

$$a_0 = \frac{\hbar}{m_e c \alpha} \quad \text{Ry} = \frac{m_e c^2 \alpha^2}{2} \quad (3.10)$$

are the Bohr radius and Rydberg energy, respectively. We chose these to set the scale because of their closeness to the atomic scale. Inserting these into the Schrödinger equation simplifies it to

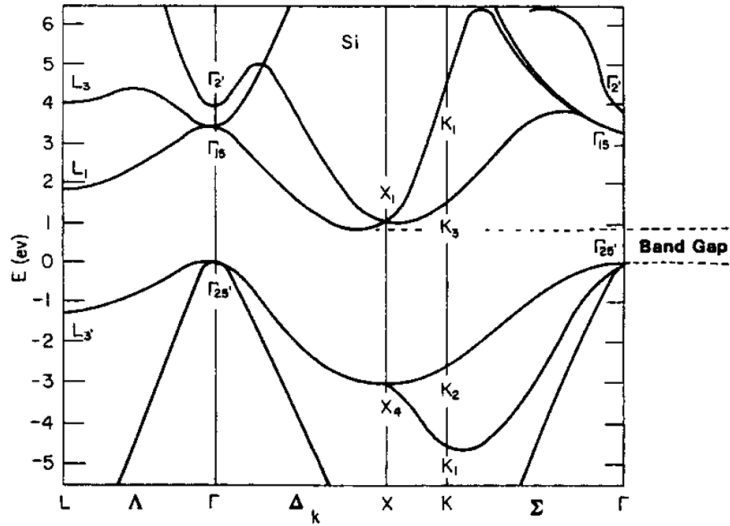
$$-\psi''(\tilde{x}) + \tilde{V}(\tilde{x})\psi(\tilde{x}) = \tilde{E}\psi(\tilde{x}). \quad (3.11)$$

Therefore, simply setting $m = 1$ and $\hbar = \sqrt{2}$ forces our units to be Bohr radii and Rydberg energies.

3.3.2 Kronig-Penney Parameters

The archetypal monoatomic semiconductor is silicon, so we chose the Kronig-Penney parameters to model it. Silicon has a lattice constant of $5.431\text{\AA} = 10.26a_0$ so we chose $\alpha = 10.26a_0$. We use the convention that the potential due to the Silicon ions would be negative, so $\alpha - a$ corresponds to the ion radius. We simply use its atomic radius which corresponds to $\alpha - a = 2a_0$. This parameter is more difficult to choose because atomic radii aren't well defined, but, at any rate, their potentials are certainly not square wells, so we are only interested in being in the ballpark. Specifying the well-depth is more complicated. Fig. 3.3. shows the band structure of Silicon. Comparing this to the Kronig-Penney band structure in Fig. 2.2. we see that the second and third band of Kronig-Penney roughly correspond to the valence and conduction bands of silicon if they were aligned in k-space. Therefore, we tuned the well depth so that the gap between the second and third Kronig-Penney bands is the same as the bandgap of silicon. $U_0 = -0.33$ Ry predicts a bandgap of 0.0824 Ry, close

Figure 3.3: The bandstructure of Silicon is fairly complicated because it's an indirect bandgap semiconductor meaning the bandgap isn't due to band edges that are aligned in k -space. However, if we imagine shifting the bands so that it was a direct bandgap material like Kronig-Penney, then the Silicon bands would most closely correspond to the second and third Kronig-Penney bands[19].



to the actual value of 0.0816 Ry. With these three parameters, the Kronig-Penney model is now completely defined. In quantum dots, electrons usually reside in the conduction band, so we use $|3, 0\rangle$ as the unperturbed state whose position space wave function is shown in Fig. 3.4. The energy of this state is 0.3587 Ry.

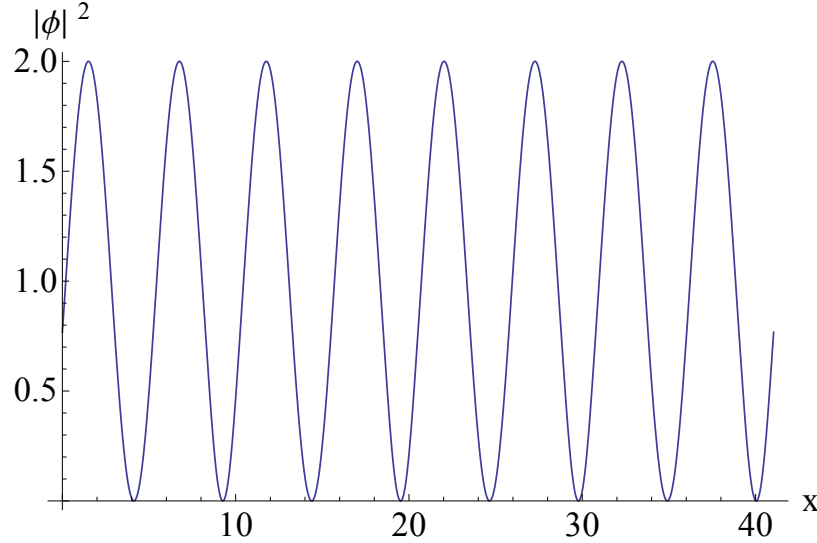
3.3.3 Perturbation Parameters

The parameters we chose for the perturbation are inspired by InGaAs quantum dots[4]. For γ we chose a typical lattice mismatch parameter for InGaAs and GaAs, in particular, we use $\gamma = 1.05$. We chose U_p to be the -0.3 eV band offset between GaAs and $\text{Ga}_{0.8}\text{In}_{0.2}\text{As}$ which implies $U_p = -0.02\text{Ry}$. Finally, we set $N_p = 20$ and $N_0 = 60$ so that the perturbation is contained in roughly one third of the system. These are fairly typical parameters for a InGaAs dot.

3.4 Results

We ran the methods in three different cases: $\gamma = 1$ and $U_p = -0.02$, $\gamma = 1.05$ and $U_p = 0$, and with both $U_p = -0.02$ and $\gamma = 1.05$. To analyze the results, we compared the predicted energies and their differences, the number of localized states, and the extent to which the wave function is confined to the perturbation. We defined this

Figure 3.4: The calculated Kronig-Penney wave function for the model over 4 unit cells. It's exactly what one would expect: a travelling wave periodic in the lattice.



last measure as

$$\frac{\int_0^{\alpha\gamma N_p} |\psi(x)|^2 dx}{\int_0^{\alpha N_0} |\psi(x)|^2 dx}. \quad (3.12)$$

We also qualitatively compared the predicted envelope and wave functions.

3.4.1 Constant Perturbation Only

Table 3.1: Results for case of constant perturbation only.

Exact						
Node	Energy (Ry)	Conf.	ΔE (Ry)			
0	0.3413	0.9635				
1	0.3481	0.8622	-0.0068			
2	0.3566	0.581	-0.0085			

EFA						
Node	Energy (Ry)	% Error	Conf.	% Error	ΔE (Ry)	% Error
0	0.341207	0.0272	0.9695	-0.0623		
1	0.348337	-0.068	0.8607	0.174	-0.00713	-4.853
2	0.357859	-0.353	0.4047	30.3442	-0.00952	-12.025

In the case of $\gamma = 1$ and $U_p = -0.02$, the EFA and EMA will return the same result because the lattices are perfectly matched so the effective mass is constant throughout

the system and the envelope-function and effective mass potentials will be identical. Both the exact method and EFA predict three localized states. The properties of these states are in Table 3.1; node refers to the number of nodes of the envelope of the wave function in the perturbed region. It is arguable that the third EFA state isn't localized because its confinement measure is less than 0.5, but we will consider it because the wave function does not attain a maxima in the unperturbed region. This wave function, and the next excited one to show they are qualitatively different, are shown in Fig. 3.5. In this case the EFA does an excellent job predicting energies, but has 4% and 12% error in predicting the energy differences. The accuracy in the overall energy, but large error in predicting the differences suggests that the energies in this regime are still dominated by Kronig-Penney. What's more interesting though, is the predictions for confinement. The EFA overestimates confinement of the first state which doesn't make sense because the EFA cuts out the higher Fourier modes of the potential, softening the boundaries. However, there is the expected result of underestimating confinement for the second and especially third excited state. It's possible this is due to error in *Mathematica*'s built in numerical integrator. To resolve this we would have to write a custom symbolic integrator.

3.4.2 Lattice Constant Perturbation Only

Table 3.2: Results for case of only perturbed lattice constant.

Exact						
Node	Energy (Ry)	Conf.	ΔE (Ry)			
0	0.3263	0.9832				
1	0.3332	0.9399	-0.0069			
2	0.3428	0.8723	-0.0096			
3	0.3534	0.7391	-0.0106			

EFA						
Node	Energy (Ry)	%Error	Conf.	%Error	ΔE (Ry)	%Error
0	0.356741	-0.09329	0.8466	0.138934		

The results for this scenario are in Table 3.2 and the corresponding wave functions are in Fig. 3.6. In this case there are several interesting results. First, is that the EMA predicts no localized states. The lack of localized states can be interpreted as a consequence of Schrödinger equation not admitting solutions with energies less than the minimum of the potential. The EFA admits only one localized state in contrast to the exact method's four. For the state it does find, it has 10% error in overestimating the energy and underestimating confinement. The confinement error is probably due to violating the assumption that the high-frequency Fourier coefficients of the perturbation are small. The energy overestimate probably reflects a band-theory version of the result that the expectation value of energy for a wave function can not be less than the ground state energy.

Figure 3.5: The top wave function is the amplitude of the third wave function predicted by the EFA in the case of only constant perturbation. It's arguable this wave function isn't strongly localized because its confinement measure is less than 0.5. Nevertheless, we count it because the wave function does not have a maxima in the unperturbed region and if the length of the unperturbed region were increased the confinement measure would also increase. The bottom wave function is the next excited state to show that the localized and non-localized wave functions are qualitatively different.

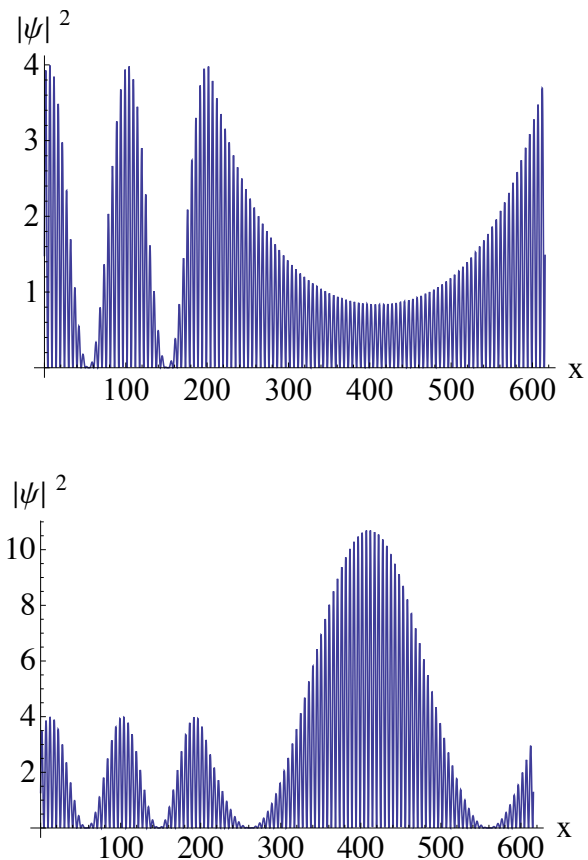
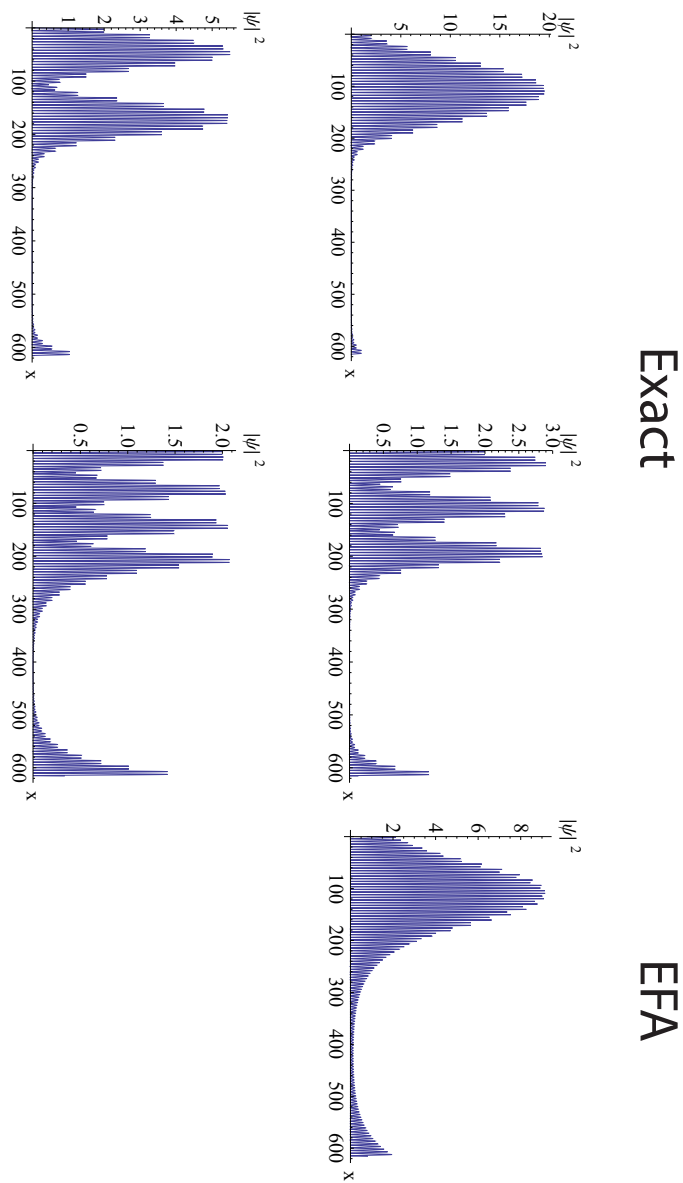


Figure 3.6: The predicted wave functions for the case of $U_p = 0$ and $\gamma = 1.05$.



3.4.3 Both Perturbations

Table 3.3: Results for case of both perturbations applied.

Exact						
Node	Energy (Ry)	Conf.	ΔE (Ry)			
0	0.3066	0.9872				
1	0.3142	0.9587	-0.0076			
2	0.3247	0.9236	-0.0105			
3	0.3369	0.8776	-0.0122			
4	0.3496	0.791	-0.0127			
EMA						
Node	Energy (Ry)	%	Conf.	% Error	ΔE (Ry)	% Error
0	0.341027	-11.229	0.9728	1.4587		
1	0.347727	-10.671	0.877	8.522	-0.0067	11.8421
2	0.357047	-9.9962	0.5303	42.5834	-0.00932	11.2381
EFA						
Node	Energy (Ry)	% Error	Conf.	% Error	ΔE (Ry)	% Error
0	0.337617	-10.116	0.9712	1.6207		
1	0.345827	-10.066	0.9032	5.7891	-0.00821	-8.026
2	0.355803	-9.579	0.6165	33.2503	-0.00998	4.9905

The data for both perturbations applied is in Table. 3.3 . In this case the exact method predicts 5 localized states to the 3 predicted by both the EFA and EMA. Both the EFA and EMA are poor at predicting energies, with both averaging around 10% error, but with the EFA doing better by about 0.75%. Again, they both are poor at predicting energy differences, but the EFA does much better than the EMA; beating it by 3% and 6%. Both the EMA and EFA do a poor job of predicting confinement, especially for excited states with the error jumping from around 5% to 35% going from the second to third state for each. By all measures except for confinement of the first state, the EFA surpasses the EMA. Select wave functions and envelope-functions for this model are in Figures 3.7, 3.8, and 3.9. The wave functions are more or less what one would expect; the ground state has a Gaussian envelope and then excited states add nodes to the envelope. One interesting difference between the envelope-functions predicted by the EFA and EMA is that the functions predicted by the EFA have oscillations on the scale of the lattice. This is due to the EFA attempting to solve a potential large, high-frequency Fourier modes.

Another interesting question is if the kinks in the wave functions predicted by the EMA can be considered as due attractive or repulsive Dirac potentials. The discontinuity in the derivative of the wave function for a Dirac potential is, in non-dimensional form,

$$\Delta\psi' = \alpha\psi, \quad (3.13)$$

where α is the strength of the Dirac spike; if it's positive, then the spike is repulsive

Table 3.4: These are the strengths of the Dirac delta potentials that kink the envelopes and wave functions of the EMA. Subscripts indicate if it's the kink of an envelope or wave function and if it's the kink at the left or right end of the perturbation.

Node	α_{Fl}	α_{Fr}	$\alpha_{\psi l}$	$\alpha_{\psi r}$
0	-0.0026	-0.0024	-0.0075	-0.0024
1	-0.0019	-0.0019	-0.0021	-0.0019
2	-0.0007	-0.0007	-0.0007	-0.0007

and vice versa[12]. The values of α are shown in Table 3.4.3. In all cases, the kinks would be caused by attractive Dirac potentials and the strength of the kink decreases with energy. The second result makes sense because at higher energies the states “see” less of the potential well. However, it’s not clear to us that all of the states would have a kink corresponding to an attractive spike. It would be interesting to explore if the sign of the spike depends on if the perturbation is the minority or majority of the system. Also, the strength aren’t the same on the left and right sides of the potential. This suggests that both the Δ region and lack of parity invariance affect the system. Finally, it’s acceptable that these effective delta potentials don’t bind states because if the Hamiltonian, Eq. 2.90, is expanded, the delta functions will have a leading momentum operator, meaning they aren’t strictly part of the potential.

3.4.4 General Comments

First, with regards to the validity of the EFA and EMA, we can conclude that for this model the EFA is superior to the EMA, and is reasonably good for when the perturbation is a constant, but suffers when a lattice constant perturbation introduces large, high-frequency, components to the perturbation. The superiority of the EFA also suggests that the quantum dots are indeed too small to be treated as bulk-materials as the EMA assumes.

There are two particularly interesting trends that all the trials shared. First, is that the EFA and EMA significantly underestimated how confined the wave functions are to the perturbation. The second is that both the EFA and the EMA underestimated the number of localized states.

The first is interesting because quantum dots are being investigated as a possible tool for increasing the efficiency of solar cells. In order for an electron in a dot to be useful, it must be extracted from the dot and my results, provided they carry over to higher-dimensional and more complicated systems, suggest that this may be more difficult than originally anticipated.

The miscounting of states is interesting because it suggests there is a deep limitation in the application of both the EFA and EMA. We suspect this is due to using the unperturbed wave functions as the basis in the perturbation expansion because they are fundamentally non-localized due to Bloch’s Theorem. An interesting project might be to try to re-work the EFA using Wannier functions, which are localized, as

Figure 3.7: These are the predicted envelope-functions of the EFA and EMA for the model with $U_p = -0.02$ and $\gamma = 1.05$. Notice how the EFA has high-frequency oscillations on top of the envelope and both exhibit less confinement as they increase in energy.

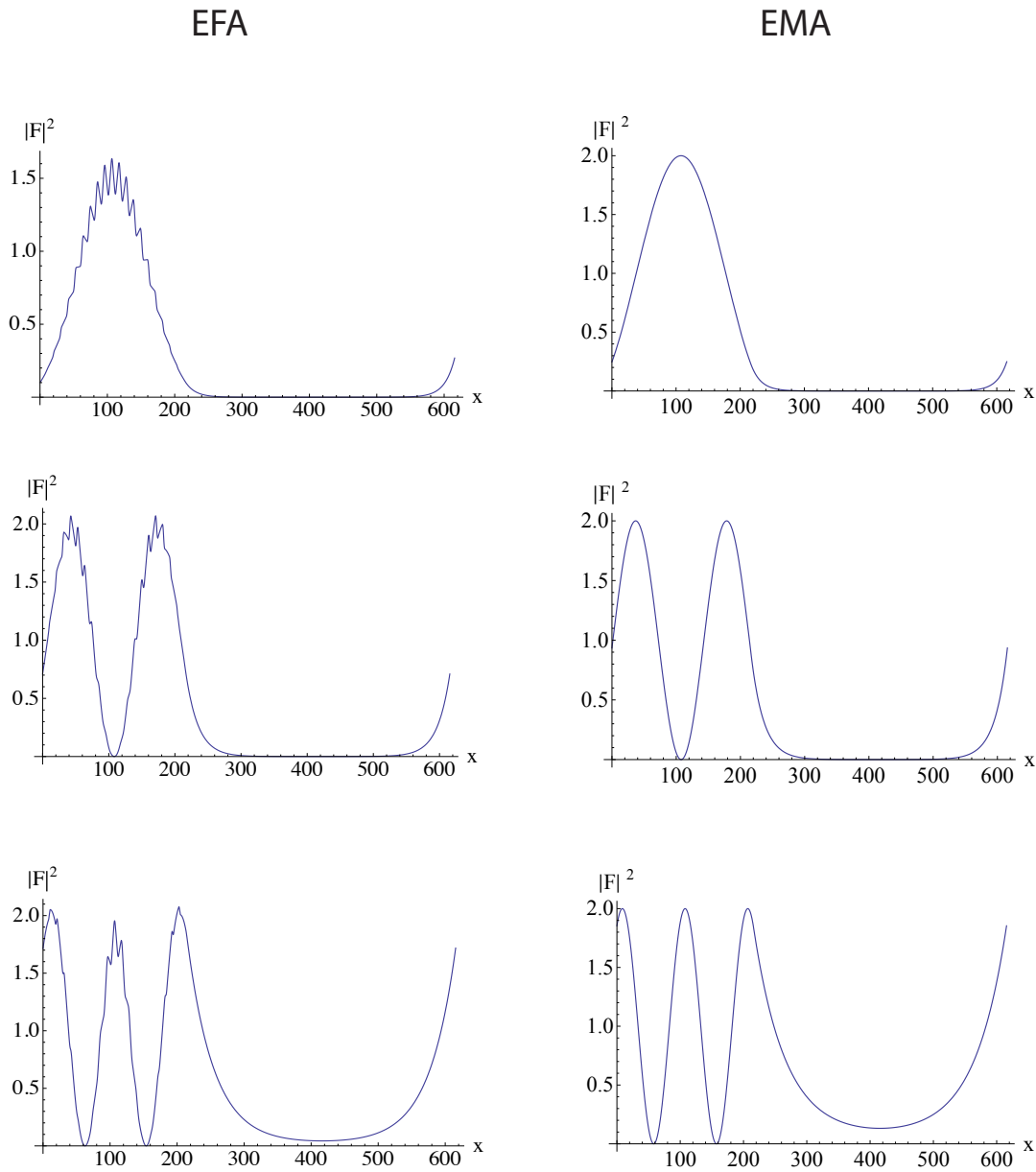


Figure 3.8: These are the shared predicted wave functions of the exact solution, EFA, and EMA for the model with $U_p = -0.02$ and $\gamma = 1.05$. Notice how with each energy increase a node in the envelope is added in the perturbed region. Also, we can qualitatively see how badly the EFA and EMA estimate confinement for the third state.

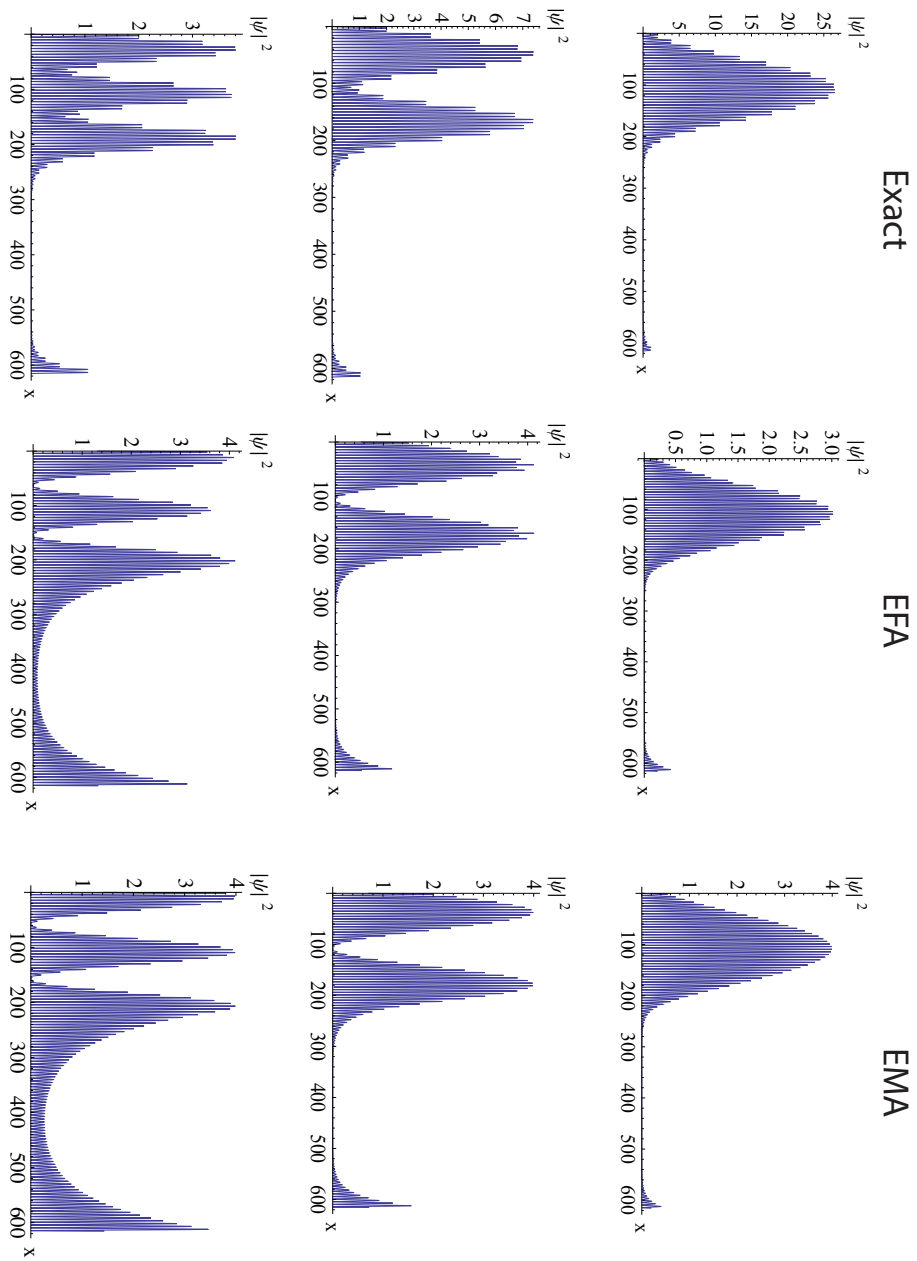
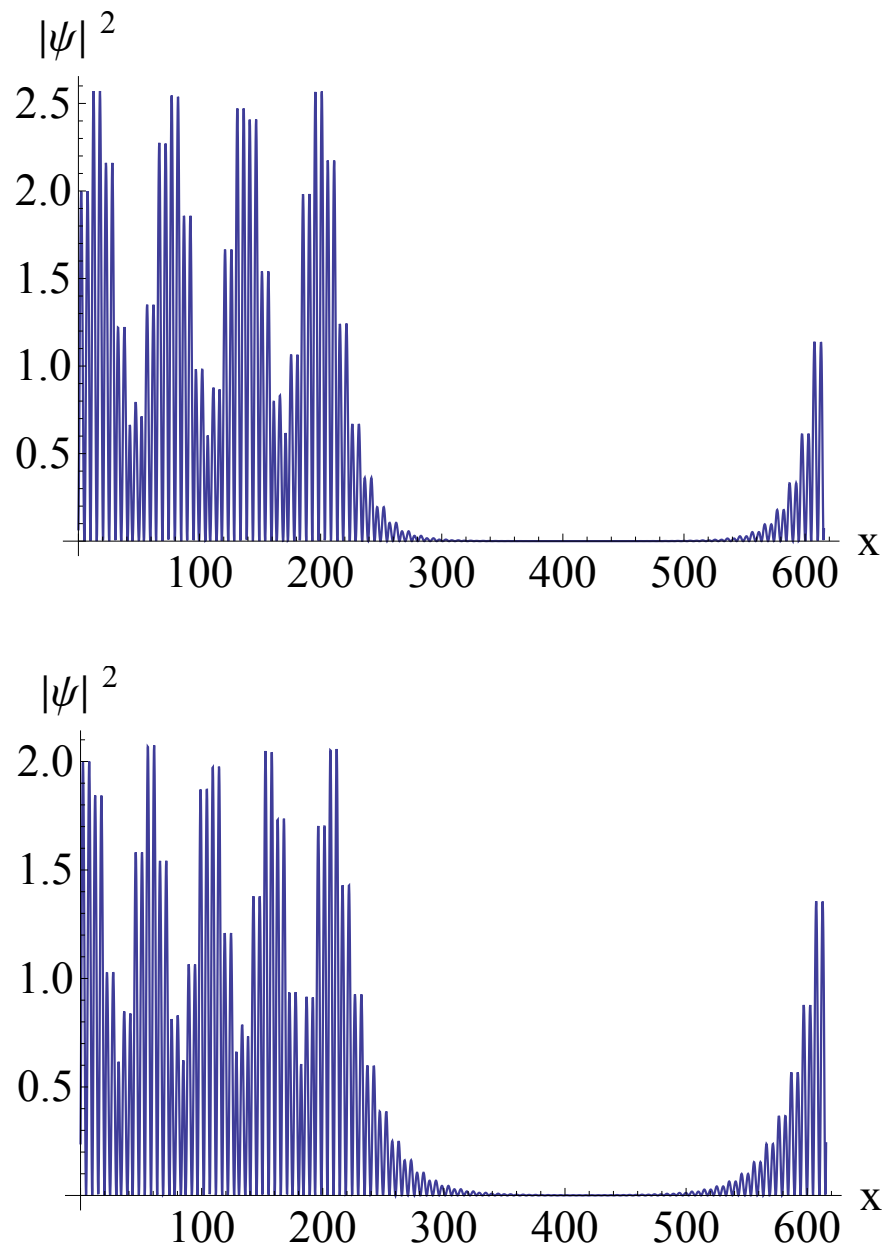


Figure 3.9: These are the higher-energy states that the EFA and EMA fail to predict. We can see how even these high-energy states are nearly as confined as the second states predicted by the EFA and EMA.



the basis states[17].

Another interesting possibility is that because the potentials for the EFA may be thought of as pseudo-random they may actually be examples of Anderson localization. Investigating this would be a significant undertaking because we're not using a tight-binding Hamiltonian[18].

Finally, in actually carrying out the above computations, we found solving the EFA was more time consuming than solving the exact method or the EMA. This was due to having to use Eq. 1.7 to calculate \mathbb{PT} . Because of it's slowness and being inherently less accurate than the exact solution, we consider the EFA totally unsuitable for solving these types of problems.

Chapter 4

Conclusion

The purpose of this thesis was to evaluate the validity of the envelope-function and effective-mass approximations. To do this, we built a one-dimensional model of a quantum dot and developed a method capable of solving it exactly. We then compared the predicted properties of the energy eigenstates between the exact solution, the EFA and the EMA.

We found that the EFA is a suitable approximation when the perturbing potential was a step function, corresponding to small high-frequency Fourier modes, but failed catastrophically when the perturbing potential changed the lattice constant, meaning it had large high-frequency Fourier modes. We also found the EFA to have generally superior results compared to the EMA, suggesting the perturbation was too small to count as a bulk material.

Two trends throughout were that the EMA and EFA underestimated the extent to which the wave function was confined to the dot and underestimated the number of localized states. The former is probably due to the EFA and EMA neglecting the higher Fourier modes of the potential, effectively softening its edges. The latter may be due to problems inherent in using non-localized wave functions as a basis for constructing localized ones.

There are several interesting ways this work could be extended. First, solving the model could be automated, making it easy to explore a much larger region of parameter space and determine what factors influence the accuracy of the EMA and EFA. Secondly, an attempt could be made to enhance the EMA and EFA. This could be done by either choosing a better basis for the wave function, or including more terms in the Taylor expansion for the energy. Finally, an attempt could be made to expand the exact method to work in higher-dimensions to analyze the effects of additional degeneracy, band overlap, etc.

Appendix A

Proof of Unimodular Matrix Power Formula

A constructive version of this argument may be found in Griffiths, Steinke, 2001[12].

The purpose of this appendix is to prove the result that if \mathbb{Q} is unimodular, then

$$\mathbb{Q}^n = \mathbb{Q}U_{n-1}(q) - \mathbb{I}U_{n-2}(q), \quad (\text{A.1})$$

where

$$U_n(q) = \frac{\sin [(n+1) \arccos(q)]}{\sqrt{1-q^2}} \quad (\text{A.2})$$

are the Chebyshev polynomials of the second kind and

$$q \equiv \frac{1}{2}Tr(\mathbb{Q}). \quad (\text{A.3})$$

This formula follows from the Cayley-Hamilton theorem and is easily proven using induction. Consider a 2×2 matrix, \mathbb{Q} , whose determinant is one. Its characteristic equation is

$$\det(\mathbb{Q} - \mathbb{I}q) = 0 = q^2 - qTr(\mathbb{Q}) + 1. \quad (\text{A.4})$$

Next, the Cayley-Hamilton theorem states matrices satisfy their own characteristic equation. Hence,

$$\mathbb{Q}^2 - 2q\mathbb{Q} + \mathbb{I} = 0 \quad (\text{A.5})$$

$$\mathbb{Q}^2 = 2q\mathbb{Q} - \mathbb{I} \quad (\text{A.6})$$

. To show $\mathbb{Q}^n = \mathbb{Q}U_{n-1}(q) - \mathbb{I}U_{n-2}(q)$, first consider the base case $n = 2$:

$$\mathbb{Q}U_1(q) - \mathbb{I}U_0(q) = \mathbb{Q}2q - \mathbb{I}(q) = \mathbb{Q}^2. \quad (\text{A.7})$$

Next, assume $\mathbb{Q}^n = \mathbb{Q}U_{n-1}(q) - \mathbb{I}U_{n-2}(q)$ to show $\mathbb{Q}^{n+1} = \mathbb{Q}U_n(q) - \mathbb{I}U_{n-1}(q)$. Multiplying both sides of the assumption by \mathbb{Q} ,

$$\mathbb{Q}^{n+1} = \mathbb{Q}^2U_{n-1}(q) - \mathbb{Q}U_{n-2}(q), \quad (\text{A.8})$$

and substituting in the result for \mathbb{Q}^2 from the Cayley-Hamilton theorem,

$$\mathbb{Q}^{n+1} = (2a\mathbb{Q} - \mathbb{I})U_{n-1}(q) - \mathbb{Q}U_{n-2}(q) \quad (\text{A.9})$$

$$= \mathbb{Q}(2qU_{n-1}(q) - U_{n-2}(q)) - \mathbb{I}U_{n-1}(q) \quad (\text{A.10})$$

Applying the recursive definition for the Chebyshev polynomials of the second kind, $U_{n+1}(x) = 2xU_n(x) - U_{n-1}(x)$,

$$\mathbb{Q}^{n+1} = \mathbb{Q}U_n(q) - \mathbb{I}U_{n-1}(q) \quad (\text{A.11})$$

completing the argument.

Appendix B

Annotated Code

There are five main types of modules I wrote to accomplish this thesis; general calculation, building and manipulating potentials, calculating $r(E)$, numerics, Kronig-Penney, and building functions. I will discuss each in a section in turn.

B.1 General Calculation

```
getk[m_, hbar_, e_, v_] := Module[{},
  Return[Sqrt[2 m (e - v)] / hbar];
]
```

This module calculates k_i given a mass, m, \hbar , hbar, energy, e, and potential, v.

```
mat1[k_, k1_, a_] := Module[{β},
  β = k / k1;
  Return[ $\frac{1}{2} \begin{pmatrix} e^{i a k} (1 + \beta) & e^{-i a k} (1 - \beta) \\ e^{i a k} (1 - \beta) & e^{-i a k} (1 + \beta) \end{pmatrix}$ ];
]
```

This module calculates the M_i . k is the k of the i^{th} , k1 is the k of the next region, and a is the length of the i^{th} region.

```
mat1eff[m1_, m2_, k1_, k2_, a_] := Module[{β, v, ret},
  β =  $\frac{m2}{m1} \frac{k1}{k2}$ ;
  v = Exp[I k1 a];
  ret =  $\frac{1}{2} \begin{pmatrix} v (1 + \beta) & 1/v (1 - \beta) \\ v (1 - \beta) & 1/v (1 + \beta) \end{pmatrix}$ ;
  Return[ret];
];
```

This creates the matrices that enforce the continuity relations for the EMA. 1's refer to quantities to the left and 2's to the right.

```
Unipower[M_, n_] := Module[{U, a, ret},
  U[x_, m_] := Sin[(m+1) ArcCos[x]] / Sqrt[1 - x^2];
  a = 0.5 Tr[M];
  Return[N[M U[a, n-1] - IdentityMatrix[2] U[a, n-2]]];
]
```

This implements the shortcut for raising unimodular matrices to an arbitrary power. I have to write out the Chebyshev polynomial in trigonometric form because *Mathematica* defaults to using the actual polynomials which is slower.

B.2 Manipulating Potentials

```
potdiff[V1_, V2_] := Module[{v1, v2, lout, uout, data, i, du, l, x, ret},
  v1 = V1;
  v2 = V2;
  data = {};
  While[Length[v1] > 0 && Length[v2] > 0,
    du = v1[[1, 2]] - v2[[1, 2]];
    If[
      v1[[1, 1]] - v2[[1, 1]] > 0,
      v1[[1, 1]] = v1[[1, 1]] - v2[[1, 1]];
      l = v2[[1, 1]];
      v2 = Delete[v2, 1];
      If[
        v1[[1, 1]] - v2[[1, 1]] < 0,
        v2[[1, 1]] = v2[[1, 1]] - v1[[1, 1]];
        l = v1[[1, 1]];
        v1 = Delete[v1, 1];
        l = v2[[1, 1]];
        v1 = Delete[v1, 1];
        v2 = Delete[v2, 1];
      ];
    ];
    data = Append[data, {l, du}];
  ];
  data = potcontract[data];
  data = delsmallpot[data];
  data = potcontract[data];
  Return[data];
]
```

This code is used to calculate the difference between two potentials. Its argument are two potentials using the convention I define in the introduction.

```

potcontract[v_] := Module[{v, i, j, k, lout, uout, v2},
  v = V;
  j = 1;
  While[j > 0,
    j = 0;
    For[i = 1, i < Length[v], i++,
      If[Abs[v[[i, 2]] - v[[i + 1, 2]]] < 10^-10,
        v[[i + 1, 1]] = v[[i + 1, 1]] + v[[i, 1]];
        v = Delete[v, i];
        j++;
      ];
    ];
  ];
  Return[v];
]

```

This module contracts a potential by combining adjacent regions with the same potential

```

delsmallpot[v_] := Module[{j, v},
  v = V;
  j = 1;
  While[j < Length[v],
    If[v[[j, 1]] < 10^-12,
      v = Delete[v, j];
      j++];
  ];
  Return[v];
]

```

One of the quirks of the implementation of the potential difference calculation is that floating point error produces a lot of regions with lengths on the order of machine epsilon. This eliminates them.

```

buildeactpot[a_, a_, u0_, y_, up_, n0_, np_] := Module[{j, del, potleft, potright, potmid, data},
  potleft = ArrayFlatten[Table[{{y a, up}, {(a - a), u0 + up}}, {i, 1, np}], 1];
  potright = ArrayFlatten[Table[{{a, 0}, {((a - a), u0)}, {i, 1, Floor[n0 - np y]}}, 1];
  del = a (n0 - np y - Floor[n0 - np y]);
  If[del > 0,
    potmid = {del, 0};
    data = Join[potleft, {potmid}, potright];
    data = Join[potleft, potright];
  ];
  Return[data];
]

```

This module generates the list of ordered pairs that correspond to the exact potential. The naming convention for arguments is the same as in the introduction.

```

buildkppot[a_, a_, u0_, n0_] := Module[{pot},
  pot = Table[{{a, 0}, {a - a, u0}}, {i, 1, n0}];
  pot = ArrayFlatten[pot, 1];
  Return[pot];
]

```

Same, but for the unperturbed potential. The potential used by the EFA is generated by subtracting these two.

```

potfunc[data_] := Module[{n, llist, val, parts},
  n = Length[data];
  llist = Table[Sum[data[[j, 1]], {j, i}], {i, 1, n}];
  llist = Prepend[llist, 0];
  val = Table[data[[i, 2]], {i, 1, n}];
  parts = Flatten[Table[{val[[i]], llist[[i]] < # < llist[[i + 1]]}, {i, 1, n}]];
  parts = Table[{parts[[i]], parts[[i + 1]]}, {i, 1, Length[parts], 2}];
  Return[parts];
];

```

This takes a potential as an argument and produces an object that can be passed to Piecewise to plot the potential. I used this to make Fig. 9.

B.3 Calculating $r(E)$

```

exacterr[a_, α_, u0_, γ_, up_, n0_, np_, e_, m_, hbar_] :=
Module[{k0, k1, k2, k3, m11, p1, m12, p2, p, del, s1, s2, T1, T2, ret},
  k0 = getk[m, hbar, e, up];
  k1 = getk[m, hbar, e, up + u0];
  k2 = getk[m, hbar, e, 0];
  k3 = getk[m, hbar, e, u0];
  m11 = mat1[k0, k1, γ a];
  p1 = mat1[k1, k0, γ (α - a)];
  m12 = mat1[k2, k3, a];
  p2 = mat1[k3, k2, α - a];
  p = mat1[k3, k0, α - a];
  del = α (n0 - np γ - Floor[n0 - np γ]);
  If[del ≠ 0,
    s1 = mat1[k1, k2, γ (α - a)];
    s2 = mat1[k3, k3, del];
    s1 = IdentityMatrix[2];
    s2 = mat1[k1, k2, γ (α - a)];
  ];
  T1 = Unipower[p1.m11, np - 1];
  T2 = Unipower[p2.m12, Floor[n0 - γ np] - 1];
  ret = Abs[Det[p.m12.T2.s2.s1.m11.T1 - IdentityMatrix[2]]]^2;
  Return[ret];
];

```

This returns $\det(\mathbb{P}\mathbb{T} - \mathbb{I})$ for the exact solution. It's simply the code version of Eq. 3.1, but starts from the basic parameters and calculates all the relevant intermediate quantities.

```

enverr[data_, e_, m_, hbar_] := Module[{n, k, M, T, j, P, Q, ret},
  n = Length[data];
  k = Flatten[Table[getk[m, hbar, e, data[[i, 2]]], {i, 1, n}]];
  M = Table[mat1[k[[i]], k[[i + 1]], data[[i, 1]]], {i, 1, n - 1}];
  T = IdentityMatrix[2];
  For[j = 1, j < Length[M], j++, T = M[[j]].T];
  P = mat1[k[[n]], k[[1]], data[[n, 1]]];
  Q = P.T;
  ret = Abs[Det[Q - IdentityMatrix[2]]]^2;
  Return[ret];
];

```

This does the same thing except for the EFA. Although it's less code than the above module, the For loop takes a long time to execute. data refers to a potential

```

effmassenv[a_, n0_, γ_, np_, up_, e_, m1_, m2_, hbar_] := Module[{k1, k2, a, L, ret},
  k1 = getk[m1, hbar, e, up];
  k2 = getk[m2, hbar, e, 0];
  a = a γ np;
  L = a n0;
  ret = 4 k1 k2 m1 m2 + (k2 m1 - k1 m2)^2 Cos[a (k1 + k2) - k2 L] - (k2 m1 + k1 m2)^2 Cos[a k1 - a k2 + k2 L];
  Return[ret];
];

```

This calculates Eq. 3.8. I chose to implement it this way so I didn't have to mess with modernizing all my code for multiple effective masses for such a simple system.

B.4 Numerics

```

bisectstart[f_, x0_, dx_, xmax_] := Module[{xl, xr},
  xl = x0;
  xr = x0 + dx;
  While[f[xl] * f[xr] ≥ 0 && xr ≤ xmax,
    xl = xl + dx;
    xr = xl + dx;
  ];
  Return[{xl, xr}]
]

```

This module finds a rough estimate for the location of a root by testing for a zero-crossing of f at points dx apart starting at x0. The program won't run forever if there aren't roots because of xmax.

```
bisection[f_, xstart_, eps_] := Module[{xl, xr, xm},
  xl = xstart[[1]];
  xr = xstart[[2]];
  While[xr - xl > eps,
    xm = 0.5 (xl + xr);
    If[f[xl] f[xm] > 0,
      xl = xm,
      xr = xm];
  ];
  Return[0.5 (xl + xr)]
]
```

This is a pretty straightforward bisection routine. `xstart` is the starting interval for rootfinding and it runs until the interval is `eps` and then returns the average of the endpoints.

```
numder[f_, x0_, dx_] := Module[{},
  Return[(f[x0 + dx] - f[x0 - dx]) / (2 dx)];
]
```

Just calculates the numerical derivative of a function at `x0` by sampling it at points `dx` away.

```
extrema[f_, x0_, dxr_, dxd_, xmax_, n_, eps_] := Module[{g, extrema, i},
  g[xs_] := numder[f, xs, dxd];
  extrema = Table[x0, {i, 1, n + 1}];
  For[i = 2, i ≤ n + 1, i++,
    extrema[[i]] = bisection[g, bisectstart[g, extrema[[i - 1]] + dxr, dxr, xmax], eps];
  ];
  extrema = Table[extrema[[i + 1]], {i, 1, n}];
  Return[extrema];
]
```

This is what I actually use to find the extrema of the functions in the previous section. It runs bisection on the derivative of `f`. `x0` is the left endpoint of the search region, `dxr` is the `dx` used in `bisectstart`, `dxd` is the `dx` used for calculating the derivative, and `n` is the number of extrema to find. It finds multiple extrema by restarting bisection `dxr` after the previous root.

B.5 Kronig-Penney

```
kp[a_, α_, U0_, e_, m_, hbar_] := Module[{Q, K, ret, b},
  b = α - a;
  Q = Sqrt[2 m (U0 - e)] / hbar;
  K = Sqrt[2 m (e)] / hbar;
  ret = ((Q^2 - K^2) / (2 K Q)) Sinh[Q b] Sin[K a] + Cosh[Q b] Cos[K a];
  Return[ret]
]
```

This simply calculates the left two terms of Eq. 2.45.

```

energies[a_, α_, U0_, k_, n_, m_, hbar_, de_, eps_] := Module[{x, targ, emax, elist, i, b},
  b = α - a;
  emax = 10^10;
  targ[x_] := kp[a, α, U0, x, m, hbar] - Cos[k (a + b)];
  elist = Table[Min[U0, 0], {i, 1, n+1}];
  For[i = 2, i ≤ n+1, i++,
    elist[[{i}] = bisection[targ, bisectstart[targ, elist[[{i-1}]] + de, de, emax], eps];
  ];
  elist = Table[elist[[{i+1}]], {i, 1, n}];
  Return[elist];
]

```

This calculates the first n Kronig Penney energies for a given wave vector, k using iterated bisection like extrema.

```

centerreffmass[a_, α_, U0_, k_, dk_, v_, m_, hbar_, de_, eps_] := Module[{e1, e2, d, me, b},
  b = α - a;
  e1 = energies[a, α, U0, k + dk, v, m, hbar, de, eps][[{v}]];
  e2 = energies[a, α, U0, k, v, m, hbar, de, eps][[{v}]];
  d = 2 (e1 - e2) / (dk^2);
  me = hbar^2 (1 / d);
  Return[me];
]

```

This module calculates numerical effective-masses. One neat thing is that because I'm working at the bottom of a band the dispersion relation is symmetric so I only need to calculate two energies; the center and one on a side. *v* is the band index and *k*, usually 0, specify the state whose effective-mass is being calculated. *dk* is how far to the side of *k* the other necessary energy is calculated.

B.6 Building Functions

```

In[250]:= getcoeff[data_, e_, m_, hbar_] := Module[{k, n, M, a, b, i, coeff, T, P, Q, j},
  n = Length[data];
  k = Flatten[Table[getk[m, hbar, e, data[[{i, 2}]], {i, 1, n}]];
  M = Table[mat1[k[[{i}]], k[[{i+1}]], data[[{i, 1}]], {i, 1, n-1}];
  T = IdentityMatrix[2];
  For[j = 1, j ≤ Length[M], j++, T = M[[{j}].T];
  coeff = Table[0, {i, 1, n}];
  P = mat1[k[[{n}]], k[[{1}]], data[[{n, 1}]];
  Q = P.T;
  coeff[[{1}]] = Eigenvectors[Q][[{1}]];
  (*coeff[[{1}]] = {1, 0};*)
  For[i = 2, i ≤ n, i++,
    coeff[[{i}]] = M[[{i-1}]].coeff[[{i-1}]];
  ];
  Return[coeff];
]

```

This module calculates the coefficients for the Kronig-Penney wave functions, EFA envelope, and exact wave function. It first calculates \mathbb{PT} from scratch and uses an

eigenvector to seed the coefficients and then reuses the M_i to get the others.

```
In[251]:= getpsipieces[data_ , e_ , m_ , hbar_ ] := Module[{cos, parts, Llist, n, k},
  n = Length[data];
  Llist = Table[Sum[data[[j, 1]], {j, i}], {i, 1, n}];
  Llist = Prepend[Llist, 0];
  k = Flatten[Table[getk[m, hbar, e, data[[i, 2]]], {i, 1, n}]];
  cos = getcoeff[data, e, m, hbar];
  parts =
    Flatten[
      Table[{cos[[i, 1]] Exp[I k[[i]] (# - Llist[[i]])] + cos[[i, 2]] Exp[-I k[[i]] (# - Llist[[i]])],
        Llist[[i]] < # < Llist[[i+1]]}, {i, 1, n}];
      parts = Table[{parts[[i]], parts[[i+1]]}, {i, 1, Length[parts], 2}];
    ];
  Return[parts];
];


```

This module builds the functions by calculating coefficients and then putting them into a structure that can be called by Piecewise. I use `#` as the variable name so they will be pure-functions which avoids a lot of variable naming/scoping problems.

```
In[253]:= effmassenvcos[a_ , a_ , y_ , up_ , n0_ , np_ , e_ , m1_ , m2_ , hbar_ ] := Module[{L, k1, k2, cos, lp},
  L = a n0;
  lp = a y np;
  k1 = getk[m1, hbar, e, up];
  k2 = getk[m2, hbar, e, 0];
  cos = Eigenvalues[matleff[m2, m1, k2, k1, L - lp].matleff[m1, m2, k1, k2, lp]][[1]];
  cos = {cos, matleff[m1, m2, k1, k2, lp].cos};
  Return[cos];
];

In[254]:= effmasspieces[a_ , a_ , y_ , up_ , n0_ , np_ , e_ , m1_ , m2_ , hbar_ ] :=
  Module[{n, L, lp, k1, k2, cos, llist, parts, k},
  n = 2;
  L = a n0;
  lp = a y np;
  k1 = getk[m1, hbar, e, up];
  k2 = getk[m2, hbar, e, 0];
  cos = effmassenvcos[a, a, y, up, n0, np, e, m1, m2, hbar];
  llist = {0, lp, L};
  k = {k1, k2};
  parts =
    Flatten[
      Table[{cos[[i, 1]] Exp[I k[[i]] (# - llist[[i]])] + cos[[i, 2]] Exp[-I k[[i]] (# - llist[[i]])],
        llist[[i]] < # < llist[[i+1]]}, {i, 1, n}];
      parts = Table[{parts[[i]], parts[[i+1]]}, {i, 1, Length[parts], 2}];
    ];
  Return[parts];
];


```

This module does the same except for building the EMA envelope function. The main difference is the additional mass and the calling of `matleff`

References

- [1] Charles Kittel. *Introduction to Solid State Physics*. John Wiley and Sons, Inc., 2005.
- [2] Victor I. Klimov, editor. *Nanocrystal Quantum Dots*. CRC Press, 2010.
- [3] Harald Ibach and Hans Lüth. *Solid State Physics: An Introduction to Principles of Materials Science*. Springer, fourth edition, 2009.
- [4] Yasushi Shoji, Katsuhiro Akimoto, and Yoshitaka Okada. Self-organized ingaas/gaas quantum dot arrays for use in high-efficiency intermediate-band solar cells. *Journal of Physics D: Applied Physics*, 2013.
- [5] M. Oloumi and C. C. Matthai. Electronic structure of ingaas and band offsets in ingaas/gaas superlattices. *Journal of Physics: Condensed Matter*, 1991.
- [6] Smita Pathak, Elizabeth Cao, Marie C. Davidson, Sungho Jin, and Gabriel A. Silva. Quantum dot applications to neuroscience: New tools for probing neurons and glia. *The Journal of Neuroscience*, 2006.
- [7] A. J. Nozik. Quantum dot solar cells. *Physica E*, 2002.
- [8] James R. Chelikowsky and Marvin L. Cohen. Nonlocal pseudopotential calculations for the electronic structure of eleven diamond and zinc-blende semiconductors. *Physical Review B: Condensed Matter and Materials Physics*, 1976.
- [9] Fausto Rossi. *Theory of Semiconductor Quantum Devices*. Springer, 2011.
- [10] John W. Wagner. Preparation and properties of bulk $\text{In}_{1-x}\text{Ga}_x\text{As}$ alloys. *Journal of the Electrochemical Society*, 1970.
- [11] M. G. Burt. The justification for applying the effective-mass approximation to microstructures. *Journal of Physics: Condensed Matter*, 1992.
- [12] David J. Griffiths and Carl A. Steinke. Waves in locally periodic media. *American Journal of Physics*, 2001.
- [13] David J. Griffiths. *Introduction to Quantum Mechanics*. Pearson, 2005.
- [14] J. J. Sakurai and Jim Napolitano. *Modern Quantum Mechanics*. Addison-Wesley, 2011.

- [15] J. Zak. Dynamics of electrons in solids in external fields. *Physical Review*, 1968.
- [16] Joel Franklin. *CompMechanics Methods for Physics*. Cambridge University Press, 2013.
- [17] Neil W. Ashcroft and David N. Mermin. *Solid State Physics*. Cengage Learning, 1976.
- [18] Michael P. Marder. *Condensed Matter Physics*. John Wiley and Sons, Inc., 2000.
- [19] Energy bands in crystals (fundamentals of electron theory) part 3. <http://what-when-how.com/electronic-properties-of-materials/energy-bands-in-crystals-fundamentals-of-electron-theory-part-3/>.